



Review on state-of-health of lithium-ion batteries: Characterizations, estimations and applications

Sijia Yang ^a, Caiping Zhang ^{a,*}, Jiuchun Jiang ^{b,c}, Weige Zhang ^a, Linjing Zhang ^a, Yubin Wang ^a

^a National Active Distribution Network Technology Research Center (NANTEC), Beijing Jiaotong University, Beijing, 100044, China

^b Shenzhen Precise Testing Technology Co. Ltd, Shenzhen, 518100, China

^c School of Electrical and Electronic Engineering, Hubei University of Technology, Wuhan, 430068, China



ARTICLE INFO

Handling editor: Zhifu Mi

Keywords:

Lithium-ion batteries
State-of-health
Battery pack
Battery management system
Practical applications

ABSTRACT

State-of-health (SOH) monitoring of lithium-ion batteries plays a key role in the reliable and safe operation of battery systems. Influenced by multiple factors, SOH is an aging path-dependent parameter, which challenges its accurate estimation and prediction. Numerous methods have been proposed for lithium-ion batteries SOH diagnostics and prognostics, but there is little discussion on how to characterize SOH. In this paper, we first review the existing characteristic parameters in defining battery SOH at cell-level and pack-level, and then propose some suggestions for SOH definitions. The impact of external influencing factors on battery degradation is introduced to lay a foundation for SOH estimation. SOH estimation methods are categorized by the parameters used to define SOH, i.e. capacity, impedance and aging-mechanism parameters. We discuss the goals of SOH monitoring and summarize its applications from short- and long-term perspectives accordingly. Finally, the challenges and future trends of battery SOH diagnostics and prognostics are thoroughly analyzed and discussed, in order to provide a comprehensive understanding for researchers and technologists.

1. Introduction

With the growing concern over fossil fuel depletion and carbon emission, renewable energy system has become the focus in both academia and industry. As a clean storage technology, lithium-ion battery has emerged as one of the most promising candidates for electric vehicles (EV) and energy storage systems (ESS). Although lithium-ion batteries have the merits of high energy/power density and wide operating temperature range (Hu et al., 2017), performance deterioration in capacity and power is inevitable. To make matters worse, electrolyte leakage and micro-short circuit may even occur, which could lead to battery failure and trigger thermal runaway (Feng et al., 2018). Catastrophic accidents have been frequently reported worldwide: the fire accident of Tesla Model S occurred during fast charging in Norway in 2016 (Wu et al., 2016b), the self-ignition of the Samsung Galaxy S10 mobile phone in 2019 (Tian et al., 2020a), and the fire accident of a parking BYD Qin Pro EV in 2020, etc. In fact, a large number of burning accidents are found to be linked with battery aging (Tian et al., 2020a). Battery performance mutations caused by electricity abuse, thermal abuse, or manufacturing defects are the main cause of thermal runaway events compared with those caused by mechanical abuse. Therefore, to

avoid such accidents and secure reliable operation, a battery management system (BMS) with the function of monitoring battery state-of-health (SOH) plays a key role.

Battery SOH indicates a point of its lifetime and evaluates the health level of the present specific performance compared with the fresh state. Unfortunately, it cannot be directly measured like the terminal voltage, making it difficult for lifetime evaluation. SOH estimation is closely related to the battery usage history. External factors like current rates (C-rates), temperature and battery operating range affect the battery aging process, eventually leading to different aging paths. Besides, minor inner defects in manufacturing would cause deviations in the aging behavior of the battery, which challenges SOH monitoring and assessing. To estimate how much energy/power a battery can now supply, most researchers use the characterization parameters such as capacity or impedance, while some use the relevant aging-mechanism parameters to monitor aspects like the number of the cyclable Li-ions (Zhou et al., 2017) or the solid phase diffusion time of Li-ions in the positive electrode (Prasad and Rahn, 2013). In a word, SOH is an estimate that derives from a series of measurements that people interpret based on their own sets of rules. It can be a quantitative or qualitative assessment of battery aging level. The overall goals of SOH monitoring include but are not limited to ensuring safe and reliable operation of

* Corresponding author.

E-mail address: zhangcaiping@bjtu.edu.cn (C. Zhang).

Acronyms	
ANN	Artificial neural network
BMS	Battery management system
CC	Constant current
CV	Constant voltage
CE	Coulombic efficiency
DoD	Depth-of-discharge
DV	Differential voltage
DVA	Differential voltage analysis
DTV	Differential thermal voltammetry
EV	Electric vehicles
ESS	Energy storage systems
EDS	Energy dispersive X-ray spectroscopy
EFC	Equivalent full cycles
EIS	Electrochemical impedance spectroscopy
EOL	End-of-life
ECM	Equivalent-circuit-model
eSOH	electrode-level state-of-health
EUE	Energy utilization efficiency
FT-IR	Fourier transform infra-red
FBG	Fibre Bragg grating
GC-MS	Gas chromatography mass spectrometry
GC-FID	Gas chromatography-flame ionization detector
GPR	Gaussian process regression
HEV	Hybrid electric vehicles
HPPC	Hybrid Pulse Power Characteristic
HI	Health indicator
IC	Incremental capacity
ICA	Incremental capacity analysis
ICP-OES	Inductively coupled plasma optical emission spectroscopy
LAM _{PE}	Loss of active material in positive electrode
LAM _{NE}	Loss of active material in negative electrode
LLI	Loss of lithium inventory
MAE	Maximum available energy
NMR	Nuclear magnetic resonance
NEDC	New European Drive Cycle
NE	Negative electrode
OCV	Open circuit voltage
PV	Photovoltaic
PE	Positive electrode
RUL	Remaining useful life
RMSE	Root mean square error
RNN	Recurrent neural network
RVM	Relevance vector machine
SOH	State-of-health
SOC	State-of-charge
SOP	State-of-power
SOE	State-of-energy
SEI	Solid electrolyte interphase
SEM	Scanning electron microscopy
SVM	Support vector machine
TEM	Transmission electron microscope
ToF	Time-of-flight
UDDS	Urban Dynamometer Driving Schedule
UPF	Unscented particle filter
XRD	X-ray diffraction
XPS	X-ray photoelectron spectroscopy

battery systems, optimizing battery control, and providing early warning.

Over the last decade, a number of reviews have been published to provide a systematic description of battery SOH monitoring or remaining useful life (RUL) prediction. Zhang and Lee (2011) overviewed the breakthroughs in the prognostics and health monitoring of Li-ion battery with emphasis on state-of-charge (SOC) estimation, current/voltage estimation, capacity estimation and RUL prediction. Waag et al. (2014) compared the strengths and weaknesses of the methods for online battery state monitoring, where SOC, capacity, impedance parameters, available power, SOH, and RUL were involved. Bercicbar et al. (2016b) explored the SOH estimation strategies for real application through experimental techniques and adaptive models. They evaluated the accuracy and described the process of developing a complete SOH estimation model (design, parameterization, implementation and validation) in detail. Xiong et al. (2018) systematically reviewed the state-of-art of the present SOH monitoring methods and divided them into experimental-based and model-based. The benefits and drawbacks of existing methods were pointed out. Lipu et al. (2018) comprehensively summarized the SOH and RUL estimation approaches for EV applications in a comparative manner. The challenges of SOH and RUL estimation methods were analyzed internally and externally. Li et al. (2019c) did a similar review on SOH estimation and lifetime prediction focusing on data-driven. Tian et al. (2019) discussed the differences between battery operations for photovoltaic (PV) systems and EV applications. And the SOH estimation methods were reviewed in terms of PV applications from the viewpoint of signal types. Tian et al. (2020a) discussed the aging reasons for lithium-ion batteries, unveiled a new contribution with a classification framework of the SOH prediction methods, and analyzed the pros and cons of each method.

Although the existing reviews are quite notable, most of them tend to focus on the specific methods of SOH estimation and the accuracy of these methods, while there is little discussion on the characterization of

SOH, which is the base for battery performance prognosis. This discussion is particularly necessary because traditional capacity-based or impedance-based definition may fail to probe the internal aging mechanisms, resulting in the incomprehensive description of the battery SOH. Moreover, current publications seldom analyze the goals and functions of SOH monitoring, that is, how the SOH estimation results can be used for health and safety management of BMS, which we believe is the core driving force for both research and industry. Also, the critical issues of how to define and how to utilize SOH for a battery pack with cell-to-cell variation remain unresolved. Therefore, this review aims to provide a novel perspective for developing cell-level and pack-level SOH diagnosis or prognosis method/algorithms. We hope that it would be beneficial for experts and scholars to better understand the trends of SOH monitoring.

The remainder of this paper is organized as follows. Section 2 describes how the review is implemented. Section 3 introduces the definition of SOH at cell-level and pack-level, and summarizes the influencing factors of battery degradation and corresponding aging behavior. Section 4 reviews the SOH estimation methods based on both traditional and novel definitions from the perspective of the source of data acquisition. Section 5 presents the goals of SOH monitoring and reviews the current applications in short- and long-term. Section 6 discusses the challenges and prospects of battery SOH diagnosis and prognosis at cell-level and pack-level, followed by conclusions in Section 7.

2. Review screening methods

This review is based on content analysis. Web of Science, IEEE Xplore, Google Scholar and Scopus were used to find the literature for the review. We used keywords such as *lithium-ion battery*, *electric vehicles*, *battery aging*, *state-of-health*, *remaining useful life*, *health monitoring*, *aging mechanisms*, and *lithium detection* to search for relevant works within the time and scope of our review. 1262 articles came out from the first

general search and 389 of the articles were sorted by analyzing the titles, abstracts, keywords, contents and the main interest of the journal. Finally, we selected 183 articles based on impact factor, citation number, and review process.

3. Definition of SOH

In this section, we first discuss the influencing factors of battery SOH and introduce the traditional definition of cell SOH. The definition of pack SOH is reviewed and a novel definition framework is proposed.

3.1. Definition of cell SOH

Battery SOH indicates a point of its lifetime. It evaluates the health level of the present specific performance compared with the fresh state. However, there is no unified definition of SOH. To evaluate the health state, most researchers use the characterization parameters such as capacity or impedance, while some employ the relevant aging-mechanism

parameters to monitor aspects like the cyclable Li-ions (Zhou et al., 2017) or the solid phase diffusion time of Li-ions in the positive electrode (Prasad and Rahn, 2013).

Induced by calendric aging and cyclic aging, and affected by internal and external factors, battery SOH deteriorates over time. Such internal factors as compacting pressure and drying time during manufacturing may cause a deviation in battery aging behavior (Baumhöfer et al., 2014; Diao et al., 2020; Lu et al., 2019). Additionally, external environmental factors, including temperature, storage SOC, C-rates, depth-of-discharge (DoD), mechanical stress, stand-by time and operating time, affect the battery aging trend and aging rate significantly. When varied external environmental conditions cause different internal states, the aging modes of the battery can be very different, exhibited variation in degradation trajectory of capacity, resistance, temperature rise, etc. The aging modes can be categorized into four groups: loss of active material in positive electrode (LAM_{PE}), loss of active material in negative electrode (LAM_{NE}), loss of lithium inventory (LLI), and kinetics degradation (Birk et al., 2017). Even under the same external conditions, different

Table 1

Observation, analytical methods and possible mechanisms under different temperatures.

Tested battery	Temperature	Observation	Analytical methods	Possible mechanisms	Refs
2Ah cylindrical LiNi _{1/3} Mn _{1/3} Co _{1/3} O ₂ /carbon	initial cycles at 60 °C then cycled at 85 °C, and 120 °C	- A moderate 7.5% loss of capacity is measured after 26 cycles at 85 °C and a 22% loss is obtained after 29 cycles at 120 °C. - Batteries cycled at 85 °C and 120 °C exhibit a strong impedance increase of 100% and 1115%, respectively.	XRD, ⁷ Li and ¹⁹ F NMR, SEM, XPS	For 120 °C: a formation of PVdF layer at the outer part of the positive electrode with diffusion and deposition on the surface of the negative electrode, and disappearance of carbonate species and an increase of inorganic species are observed.	Boden et al. (2013)
3.07Ah 18650 LiNi _x Co _y Al ₂ O ₂ /carbon	25 °C, 60 °C	The cells that cycled using the CC protocol exhibit a much higher capacity degradation rate at 25 °C than at 60 °C.	EIS, EDS, SEM, XPS, FT-IR	- For 25 °C: Thick secondary SEI on the anode has a large resistance and different chemical composition as compared to that of 60 °C cells. - The reduction product on the anode surface at 60 °C is mostly the result of CO ₂ while the reduction product at 25 °C has more F content.	Wang et al. (2019)
114Ah prismatic LiNi _{0.5} Co _{0.2} Mn _{0.3} O ₂ /graphite	25 °C, 35 °C, 45 °C, 50 °C, 55 °C	The temperature has little effect on capacity degradation.	Half-cells	- 25 °C: LLI is the main cause in the pre-decline process, LAM _{NE} dominates later - 35–55 °C: LLI is the reason for the capacity decline.	Jia et al. (2020)
40Ah pouch Li(NiMnCo) ₂ O ₂ /graphite	Room temperature, 45 °C, 45/65 °C (cha/dch)	- The capacity fade of the 45/65 °C cell shows a different, steeper slope compared with the room temperature and 45 °C cells, but no sudden drops in capacity are observed. - The polarization resistance of the room temperature and 45 °C cells are almost equal during cycling, whereas the 45/65 °C cell shows a significantly larger polarization resistance that increases drastically after 500 cycles.	EIS, XRD, SEM, EDS, ICP-OES	- SEI-layer growth and lithium plating are attributed to be the main mechanisms responsible for capacity loss (verified by cell disassembly). - The ohmic resistance growth is attributed to the lack of electrolyte and increased separator resistance.	Jalkanen et al. (2015)
580 mAh prismatic LiFePO ₄ /graphite	25 °C, 35 °C, 45 °C, 55 °C	The ambient temperature has a strong impact on the capacity fade rate. The capacity fade rate of the full cell is accelerated with increased ambient temperature.	XRD, SEM, TEM, XPS, EDS, GC-MS, GC-FID	- Room temperature: the irreversible loss of active lithium due to the generation and reformation of SEI film while the performance decay of the cathode electrode is not distinct. - Temperature exceeds 35 °C: the enhanced electrolyte decomposition accelerates the consumption rate of active lithium.	Sun et al. (2017)
1.5Ah 18650 Li _x Ni _{1/3} Mn _{1/3} Co _{1/3} O ₂ +Li _y Mn ₂ O ₄ /graphite	-20 °C, -10 °C, 0 °C, 25 °C, 50 °C, 60 °C, 70 °C	The tested cells exhibit the slowest aging under 25 °C. For higher temperature, the aging rates rise with increased temperature. For lower temperature, the aging rates rise with decreased temperature.	SEM, EDS, ICP-OES, XRD	- Temperature below 25 °C: lithium plating and subsequent reaction with the electrolyte. - Temperature above 25 °C: degradation of the cathode and SEI film growth on the anode.	Waldmann et al. (2014)

aging trends were observed for different battery types (Jia et al., 2020; Sun et al., 2017).

Tables 1–4 elaborate typical representative references for the four commonest influencing factors of cyclic aging. By revealing their effects on battery aging paths, we hope to provide a link between the external behavior and internal mechanisms under different environmental influencing factors. We focus on the traditional lithium-ion battery with a graphite anode, and novel anode materials like lithium titanium oxide and Li metal are not included in this review. It can be seen from Table 1 that in most cases, compared with room temperature, high temperature or low temperature tends to shorten the service life of the battery. Low temperature limits the kinetics of the battery and might result in lithium plating, which could lead to accelerated LLI. Thick secondary solid electrolyte interphase (SEI) film and the loss of active material might be a contributor to the increased degradation at high temperature (Waldmann et al., 2014). However, there are also some exceptions: it was found that the temperature in the range of [25 °C, 55 °C] had little impact on the capacity degradation (Jia et al., 2020), and accelerated fading was observed at room temperature compared with high temperature (Wang et al., 2019). A large C-rate is likely to enlarge the capacity degradation rate because of the rapid deintercalation and intercalation, which might cause the structure of the active material and the layer of SEI to shatter (Sun et al., 2018). Nevertheless, some “seemingly” abnormal phenomena occur as shown in Table 2. For example, the degradation speed was lower under the C-rate of 3C compared with that of 1.5C (Guan et al., 2014). These “seemingly” abnormal phenomena are more prominent for cycling conditions of different SOC ranges. Table 3 summarizes the aging experiments of different SOC ranges or DoD and the possible aging mechanism. Saxena et al. (2016) found that a low mean SOC that less than 50% would cause slower cell degradation, while Ecker et al. (2014) concluded that the optimum range was around 50% mean SOC, and cycling around higher or lower SOC would accelerate degradation. Ecker et al. (2014) believed that crossing transitions between the voltage plateaus of the negative electrode were the reason for the faster degradation in higher or lower SOC. Compared with the other three factors, there is little literature on the influence of external compaction stress on battery aging (Table 4). It

was reported that moderate stress was beneficial to battery service life (Barai et al., 2017; Cannarella and Arnold, 2014a).

It can be summarized from these tables that the aging of lithium-ion batteries is strongly path-dependent and affected by numerous factors. The aging trajectory varies remarkably for different chemistry materials and even for the same chemistry materials, making SOH monitoring a challenging task. To analyze the aging mechanisms, post-mortem techniques and non-destructive methods have been employed. The former include scanning electron microscopy (SEM), X-ray diffraction (XRD), energy dispersive X-ray spectroscopy (EDS), and X-ray photoelectron spectroscopy (XPS) etc., and the latter generally refer to the incremental capacity analysis/differential voltage analysis (ICA/DVA) or electrochemical impedance spectroscopy (EIS) which are based on the measurable external electrical signal. However, the information provided by the traditional electrical signal is rather limited. It is shown that compared with force-based or temperature-based signal, electrical-based signal demonstrated a slower response in detecting thermal runaway (Koch et al., 2018). Therefore, for a comprehensive diagnosis, other signals like temperature or expansion need to be included to monitor other aspects of the battery as a way to hopefully prevent severe accidents from occurring.

To quantify the battery SOH, two traditional definitions based on capacity and impedance are commonly used, displayed in Eqs. (1) and (2) respectively. Eq. (1) presents battery energy capability, while Eq. (2) reflects power capability. The capacity-based definition is generally applied in EV, PV and ESS where the energy storage capability outweighs the power capability, while the impedance-based definition is more favorable in the application of hybrid electric vehicles (HEV) since the battery power performance is the main focus.

$$SOH_E = \frac{C_{aged}}{C_{fresh}} \times 100\%. \quad (1)$$

$$SOH_P = \frac{R_{EOL} - R_{aged}}{R_{EOL} - R_{fresh}} \times 100\%. \quad (2)$$

where C_{fresh} is the nominal capacity at a certain C-rate when the battery is at the fresh state, C_{aged} is the aged capacity under the same C-rate,

Table 2
Observation, analytical methods and possible mechanisms under different C-rates.

Tested battery	Current Rate	Observation	Analytical methods	Possible mechanisms	Refs
580 mAh prismatic LiFePO ₄ /graphite	1C, 2C, 3C, 4C, 5C (@25 °C)	The acceleration is enhanced obviously as the discharge rate is raised from 0.5C to 3.0C. However, when the discharge rate is higher than 3.0C, the accelerating effect on the capacity fade is not evident.	XRD, XPS, SEM	- Low current rates: irreversible loss of active lithium due to the generation of SEI film on the anode. - C-rates greater than 3C: the loss of active lithium and loss of active materials due to structure decay, the unstable and broken SEI film caused by rapid extraction of lithium-ions.	Sun et al. (2018)
1.15 Ah prismatic LiCoO ₂ /mesocarbon microbeads	0.6C, 1.2C, 1.5C, 1.8C, 2.4C, 3.0C(@25 °C)	The effect of accelerating is remarkable when the C-rates increased from 0.6C to 1.2C. The capacity retention trends are almost the same for C-rates larger than or equal to 1.5C, the degradation under 2.4C or 3.0C is even a little slower than that under 1.5C.	SEM, XRD, half-cell tests: residual capacity and ICP-OES	- The capacity deterioration is mainly caused by the decay of the reversible capacity of LiCoO ₂ cathode, the irreversible loss of active lithium and the lithium remaining in the anode. - The capacity fade of the active materials at a low rate is more obvious than that at a high rate.	Guan et al. (2014)
5Ah 32650 LiFePO ₄ /graphite	0.3C, 0.5C(@-10 °C, -20 °C)	The decay rate of 0.3C@-10 °C is the slowest, 0.5C@-10 °C takes the second place, and 0.3C@-20 °C is the fastest.	ICA	- The destruction and reconstruction of SEI film at low temperature cause the internal resistance to decrease. - The main cause of low-temperature aging is lithium plating.	Wu et al. (2020)
3.36Ah pouch LiCoO ₂ /graphite	0.7C, 1C, 2C (@10 °C, 25 °C, 45 °C, 60 °C)	The capacity degradation is found to be independent of the discharge C-rate in the range of 0.7C~2C at 10°C~45 °C. At 60 °C, cells cycled at 2C degrades much faster than those cycled at lower discharge C-rates.	EIS	- Lithium in the particle maintains nearly a homogeneous distribution at different discharge C-rates at 10°C~45 °C. - For 60 °C: Electrolyte thermal decomposition.	Diao et al. (2019b)

Table 3

Observation, analytical methods and possible mechanisms under different SOC ranges.

Tested battery	SOC ranges (@ambient temperature)	Observation	Analytical methods	Possible mechanisms	Refs
20Ah pouch Li(NiMnCo) O ₂ /graphite	1. Mean SOC 50%(@25 °C): 0–100%, 10–90%, 25–75%, 40–60% 2. 50% DoD(@35 °C): 40–90%, 25–75%, 10–60%	- Cells cycled at DoD-levels greater than 65% tends to reach the end-of-life (EOL) faster than those at smaller cycle depths. The difference between small DoD is not distinct. - Faster cell degradation occurs at elevated mean SOC.	none	Not mentioned	de Hoog et al. (2017)
1.5Ah pouch LiCoO ₂ / graphite	1. Mean SOC 50%: 0–100%, 20–80%, 40–60% 2. 60% DoD: 0–60%, 20–80%, 40–100% Both cycled @25 °C	- For the first 500 equivalent full cycles (EFC) mean SOC is found to have a major effect on the capacity fade of cells as compared to Δ SOC. However, towards the end of the testing (600–800 EFC) Δ SOC becomes the major factor affecting the capacity loss rate of the cells. - Lowering the mean SOC reduces the rate of degradation.	none	- A new degradation mechanism is activated after 500 EFC for 0–100%. - For the 0–60% range, either the absence of a degradation mechanism is present in other SOC ranges or it presents a different degradation mechanism with a very slow degradation rate.	Saxena et al. (2016)
400 mAh 18650 LiAl _{0.10} Ni _{0.76} Co _{0.14} O ₂ / graphite	1. 0–100%, 10–70% (@25 °C, 60 °C) 2. 0–60%, 10–70%, 40–100%(@25 °C)	- The capacity fade in the 0–100% range is significantly large compared to that in the other restricted DoD conditions. There is little difference in degradation behavior of discharge capacity among the three restricted 60% DoD conditions.	EIS, XRD, SEM, XPS	- Deterioration of active materials occurred in a specific potential region; the Crystal structure of active materials is destroyed in large DoD conditions. - Large DoD induces the generation of micro-crack in the cathode particles.	Watanabe et al. (2014)
2.5Ah 18650 Li(NiCoAl) O ₂ /graphite	20–50%, 35–65%, 65–95%, 20–95% (@25 °C)	After 300 EFC, the discharge capacities of cells 20–50%, 35–65%, and 65–95% ranges are reduced by 8.9%, 6.7%, and 5.9%, respectively. Cell 20–95% went through 525 EFC and its discharge capacity is reduced by 7.2%.	EIS, SEM, EDS	The generation of microcracks on the surface of the particles may be another cause of LAM _{PE} .	Benavente-Araoz et al. (2020)

Table 4

Observation, analytical methods and possible mechanisms at various mechanical stresses.

Tested battery	Mechanical Stress	Observation	Analytical methods	Possible mechanisms	Refs
90 mAh pouch Material not given	0, 15 MPa, 17 MPa, 30 MPa	As the compressive stress increases, the internal resistance and capacity loss increase.	EIS, SEM	Stress-induced pore closure and limited ionic transport.	Peabody and Arnold (2011)
500 mAh pouch LiCoO ₂ / graphite	0, 0.05 MPa, 0.5 MPa, 5 MPa	The unconstrained cells exhibit a higher rate of capacity fade than the low stack pressure cells after about 1000 cycles. Light stack pressure is beneficial to long term performance by preventing layer delamination. The standard deviation of high stack pressure is much larger than the other conditions.	SEM	Loss of cyclable lithium, film coverage.	Cannarella and Arnold (2014a)
15Ah pouch Li (NiMnCo)O ₂ / graphite	0, 5 psi, 15 psi (Pounds per square inch)	The capacity drop trend is identical for all three conditions for the first 450 cycles. After 450 cycles, the cells without any external pressure exhibit a higher capacity drop compared to the cells under pressure.	EIS	- Slower SEI growth under additional pressure. - Improved wettability of the active materials.	Barai et al. (2017)

R_{fresh} is the initial internal resistance at the fresh state, R_{EOL} is the internal resistance at end-of-life (EOL), and R_{aged} is the aged internal resistance measured or estimated at a certain time.

However, battery degradation is not always accompanied by the resistance increase (Sarasketa-Zabala et al., 2015) or capacity decline (Lucu et al., 2020), especially in the early stage of life. A “silent” effect may occur inside the battery, which means the loss of active materials may not be immediately reflected in the loss of battery capacity (Anseán et al., 2017; Dubarry et al., 2020). Fig. 1 shows the matching relationship of the positive electrode (PE) and the negative electrode (NE) with respect to the full cell SOC at the fresh and aged states. As can be seen from Fig. 1, the measurable capacity of the battery remains unaltered

even with 20% LAM_{NE}, that is to say, the capacity fade may not be observed instantly when the active material of the negative electrode is excessive. Traditional SOH definition may fail to probe the internal aging mechanisms and some conclusions draw from the external performances like capacity or impedance may even contradict each other if the internal mechanism is not analyzed in detail.

Hence, the traditional SOH definition based on a single feature is not sufficient to comprehensively characterize the battery aging level (Dubarry et al., 2020). We believe that the SOH should be defined in a broad sense, including parameters related to the aging mechanisms. So it is necessary to establish a SOH-related parameter matrix in future research work for monitoring the possible internal changes and ensuring

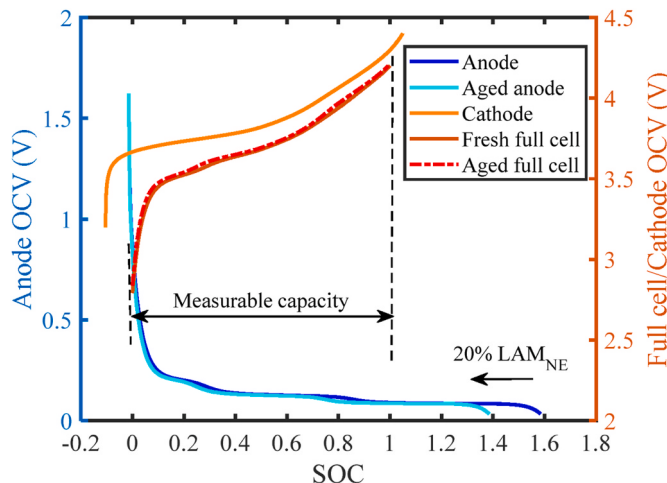


Fig. 1. “Silent” effect of battery measurable capacity.

reliable battery operation.

3.2. Definition of pack SOH

Comparatively, the definition of SOH for battery packs has not been discussed as frequently as that of the cell SOH. Table 5 summarizes the calculation methods of battery pack SOH. To be more specified, Bi et al. (2016) treated the entire battery pack as a whole and modeled it using a second-order equivalent-circuit-model (ECM). The battery pack SOH is calculated based on the change of internal resistance derived from ECM, demonstrated as Eq. (3). Hua et al. (2015) and Cordoba-arenas et al. (2015) defined the pack capacity SOH considering grouping and balancing approaches. Pack power SOH using equivalent resistance is also considered as a system-level SOH element (Eq. (4)).

Diao et al. (2017) proposed a novel SOH concept, which is defined as the ratio of the current maximum available energy of the pack to that of the original rated energy. The current maximum available energy of a single cell in the battery pack is calculated using the average open circuit voltage (OCV) when the battery is charged from 0% to 100%. They claimed that this SOH defined by energy has an advantage over the traditional SOH defined by capacity or impedance in depicting the actual state of the battery pack because it incorporates the aging of the capacity and impedance and also cell-to-cell variation. Zhang et al. (2018) defined the SOH using the maximum available energy as Eq. (5) shows except that they adopted the OCV to SOC integration instead of the average OCV of entire SOC ranges to calculate the remaining discharge energy and maximum charge energy.

$$SOH = \frac{R_{EOL} - R_{now}}{R_{EOL} - R_{new}} \times 100\% \quad (3)$$

Table 5
Equation summary of battery pack SOH calculation methods.

Equation number	Variable meaning	Refs
(3)	R_{EOL} is the resistance when battery reaching EOL (assumed $R_{EOL} = 1.6 \cdot R_{new}$), R_{now} is the current ohmic resistance, and R_{new} is the original ohmic resistance.	Bi et al. (2016)
(4)	$SOH_{C,j}$ is the capacity SOH of the j th cell, $SOH_{R,j}$ is the power SOH of the j th cell.	Cordoba-arenas et al. (2015); Hua et al. (2015)
(5)	$E_{MES,bat}(j)$ is the maximum energy storage of j th at the present state, and $E_{MES,0}(j)$ is the maximum energy storage of j th at the fresh state.	Diao et al. (2017); Zhang et al. (2018)

$$SOH_{C,pack} = \min_{1 \leq j \leq N_s} (SOH_{C,j})$$

$$SOH_{R,pack} = \max_{1 \leq j \leq N_s} (SOH_{R,j}) \quad (4)$$

$$SOH = \frac{\sum_{j=1}^{N_s} E_{MES,bat}(j)}{\sum_{j=1}^{N_s} E_{MES,0}(j)} \times 100\% \quad (5)$$

The focus of the individual cell and battery pack is different to some extent. In the practical applications of the battery-powered system, large-scale lithium-ion battery packs are equipped, composed of multiple individual cells connected in series and/or parallel to meet energy or power requirements. All these factors, such as temperature gradient (Klein et al., 2016; Paul et al., 2013), uneven current distribution (Pastor-Fernández et al., 2017), variances from the cell manufacturing process (Baumhöfer et al., 2014) etc., can lead to the inconsistency in cell performance, resulting in a deterioration of pack performance and be reflected in the battery pack SOH. Therefore, apart from the definition from an absolute value angle like the maximum available energy a pack could deliver, we believe that the relative value among the individual cells should also be included in the battery pack SOH matrix because it describes the variation degree of individual cells in the battery packs. Eqs. (6) and (7) display the range and variance of the single cell parameters in the battery pack, respectively. The single cell parameter is presented by variable X , and its average at aged state and fresh state are shown in Eq. (8). These cell-level parameters include but are not limited to integral feature such as capacity, energy, or the point feature of resistance, OCV, and terminal voltage at a certain SOC.

$$SOH_{Dif} = \frac{X_a^{\max} - X_a^{\min}}{X_f^{\max} - X_f^{\min}} \times 100\% \quad (6)$$

$$SOH_{Var} = \frac{\sum (X_{a,i} - \bar{X}_a)^2}{\sum (X_{f,i} - \bar{X}_f)^2} \times 100\% \quad (7)$$

$$\bar{X}_a = \frac{\sum X_{a,i}}{k}, i = 1, 2, 3, \dots, k$$

$$\bar{X}_f = \frac{\sum X_{f,i}}{k}, i = 1, 2, 3, \dots, k \quad (8)$$

where X_i is the specified parameter of the i th cell, k is the number of the single cells in series. The superscript max and min mean the maximum value and minimum value in the pack, and the subscript f and a denote the fresh and aged state, respectively.

4. Methods of lithium-ion battery SOH estimation

There are many ways to classify SOH estimation methods. These classification criteria inevitably differ slightly from each other, and may even overlap in some perspectives. For example, the model-based method is categorized into the branch of the experimental technique (Berecibar et al., 2016b), while it has the same status as the experimental method (Xiong et al., 2018). As a result, it may be confusing due to the overlap of certain attributes of the naming rules and is not conducive for researchers to have an in-depth understanding.

In this section, SOH estimation methods both for individual cells and battery packs are summarized. The classification is presented based on the definition of SOH, that is, the parameters to characterize. The methods of obtaining these characterization parameters are demonstrated from the perspective of the source of data acquisition sources. In addition, a scheme for battery pack SOH estimation is summarized based on the review of the current literature.

4.1. For individual cell

The characterization parameters of individual cell SOH estimation methods can be divided into three categories, (1) capacity, (2) impedance, and (3) aging-mechanism-based parameters. Although some “new” indicators that can be used for SOH monitoring have been proposed (Ansean et al., 2019; Wu and Jossen, 2018; Xia and Qahouq, 2018), they have essentially no differences with battery capacity. Therefore, instead of being classified as other health-related parameters, these references are classified into the first category: “based on capacity”. Then the SOH diagnostics or prognostics problem is transformed into battery specific parameter estimation and its trend prediction.

4.1.1. Based on capacity

Battery capacity is one of the most common parameters to describe SOH. Battery capacity loss can be directly measured by charging or discharging the battery at the nominal current to the cut-off voltage in the laboratory. Nevertheless, this procedure can hardly be performed in practice due to the limitation of apparatus and battery operation range. Therefore, in-situ battery capacity estimation methods have attracted great attention. Many scholars attempted to estimate battery capacity using parameters extracted from voltage/current/temperature signals because they are the most accessible measurements in BMS. Together with the estimation methods based on these traditional signals, novel capacity estimation methods based on other signals are also demonstrated. The SOH refers to battery capacity if not specified in the following sub-sections.

4.1.1.1. Voltage-based. Battery OCV-SOC relationship reflects unique thermodynamic information of each battery chemistry and structure, and can be used for SOH estimation (Dubarry et al., 2020). However, OCV requires a long period of resting to obtain, which is impractical for on-board application. Terminal voltage, as the most direct parameter related to OCV, has been widely used for SOH estimation. On-board techniques for SOH estimation based on voltage signal have thoroughly reviewed by (Waag et al., 2014), (Berecibar et al., 2016b), (Farnmann et al., 2015), and (Wang et al., 2020). However, they seldom summarize the methods from the perspective of the range of voltage, which determines the feasibility in practice. Therefore, this sub-section focuses on reviewing the methods from the perspective of the voltage data range used in capacity estimation.

Require to be fully charged: Lu et al. (2014) extracted three geometrical features from the charging current curve of the constant voltage (CV) stage and one from the discharging voltage curve of the constant current (CC) stage after a complete charge for capacity estimation. The Laplacian Eigenmap is adopted to construct an intrinsic manifold and the geodesic distance is calculated for battery capacity estimation. Yang et al. (2018b) extracted four geometrical features from the CCCV process (i.e. time of CC duration, time of CV duration, the slope of the curve at the end of CC charging, and vertical slope at the corner of the CC charging curve) and input them together with SOH into the Gaussian Process Regression (GPR) model for training. Half of the total datasets were used for training and a half was used for testing. The robustness was verified by an aging case under dynamic profile. Yang et al. (2018d) derived the expression of the current time constant of the charging CV stage based on a first-order ECM and correlated it with the normalized capacity to represent the SOH.

Require to be fully discharged: Wu et al. (2016a) used the terminal voltage and its changing rate with time extracted from a charging period whose range is about 0%–60% SOC to estimate SOH. The relationship between the extracted features and the battery capacity is established by a group method of data handling polynomial neural network. Severson et al. (2019) also applied machine-learning tools to predict cells’ life using features extracted from discharge voltage curves, which directly employed it for cycle life prediction rather than SOH. Yu et al. (2017)

made a contribution to finding the indirect health indicators (HIs) of a battery capacity under the randomized loading conditions. The whole storage capacity, the mean value of all internal resistance and the number of cycles at each random discharging cycle are extracted and normalized to [0,1] to establish a linear regression model for SOH estimation. Their intention is good but the extracted HIs rely on a complete discharging process (from 4.2V to 3.2V) and the method needs to be verified on a partial randomized use since the situation is rare in practice where batteries can be fully exhausted or fully charged.

However, those methods mentioned above require the battery to be fully charged (CV process) or fully discharged (discharge to cut-off voltage) more or less, which is hard to be achieved in practice at a pack level. Thus, many efforts have been made to estimate the capacity based on the middle interval of the charging or discharging process. For instance, Klass et al. (2014) trained the Support Vector Machine (SVM) with four types of datasets and input the generated hypothetical voltage response to estimate SOH. The training datasets include instantaneous voltage drop, resistance calculated by the 10s voltage drop at 90%, 70%, 50%, 30% SOC at different temperature levels, and capacity of voltage ranges from 3.0V to 4.1V (around 30%–90% SOC). Xiong et al. (2019) selected the charge capacity calculated by the ampere-hour counting within a fixed voltage range (3.6V–4.2V) as a HI. They used a third-order polynomial model to demonstrate the relationship between HI and the reference capacity at different aging states. Richardson et al. (2019) proposed a data-driven in-situ capacity estimation method employing GPR, which achieved less than 3% root mean square error (RMSE) using a partial charging voltage section of a duration of 1450s (current rate 1C, starting at 3.7V). Zheng et al. (2019) constructed a linear capacity estimation model for EV application based on the scaling of fresh and aged charging curves. The optimal fixed voltage window for capacity estimation ranged from 3.84 to 4.06 V (SOC range was approximately 25%–70%) to 3.91–4.07 V (SOC range was around 65%–85%) for different experimental conditions. Guo et al. (2014) employed a first-order ECM to characterize the constant charging portion of the charging curve and transformed it into a time-based parameter to estimate the SOH by fitting the charging voltage. However, the specific voltage range of the constant charging profile used for model fitting is not mentioned. Based on their works, Bian et al. (2020) further improved the first-order ECM and derived an open-circuit-voltage-based model whose parameters (including the SOH) were identified by fitting part of the voltage-capacity curve on the CC process. The effect of voltage window size and location of the partial CC profile was also investigated. They concluded that the adopted voltage window should include all four or most of the incremental capacity peaks, meaning that the charging or discharging profile had to cover more than 85% of the battery capacity to yield desirable results. Naha et al. (2020) collected the difference of 10 derived voltage values (Δv_{sei}) from the partial CC charging process together with the average temperature during charging to form the feature vector of Artificial Neural Network (ANN) for capacity loss estimation. Although the problem of data acquisition for methods based on middle voltage interval is alleviated to some extent, the challenge for pinpointing the underlying aging mechanisms still remains. In addition, some of the methods directly extract a portion of the voltage section from the complete charging voltage curve for establishing and validating, while the accessible voltage in practice might be different due to the polarization at different initial charging states (Jiang et al., 2020). The low data precision is another issue that needs to be dealt with. The robustness and reliability of the methods under sensor bias need further validation.

Apart from the estimation method based on the partial voltage section, another technique frequently adopted for SOH estimation is the derivative of the voltage-capacity curve: incremental capacity (IC)/differential voltage (DV) curve. Primarily used for degradation diagnosis, IC/DV curve has advantages in SOH monitoring. This is because it transforms the hard-to-decipher voltage variation into easy-to-identify peaks or valleys corresponding to the electrochemical reactions, which

vary along with degradation and can be used as characteristic parameters. Generally, the quantitative relationship between the extracted parameters and SOH are established offline. Once the specific parameters are detected from the online charging process, then the SOH can be calculated. For example, Ansean et al. (2019), Berecibar et al. (2016a) and He et al. (2020a) directly associated the intensity reduction, position shift or area of the IC or DV peaks with capacity fade. Mathematical functions were used to fit the profiles of IC peaks in (Bian et al., 2019; He et al., 2020b; Li et al., 2016; Torai et al., 2016), and the function parameters or the integral of the specific function were employed to estimate the capacity. These characteristic parameters are typically derived from charging since the charging is usually more controllable compared with volatile discharging. Some also require a complete CC charging and discharging to obtain the pseudo-OCV. The current rates employed to obtain the IC/DV curve are 0.05C (Ansean et al., 2019; Li et al., 2016), 0.2C (Torai et al., 2016), 0.3C for LiFePO₄ (Bian et al., 2019), and 0.75C for Li(NiCoAl)O₂ (He et al., 2020b), respectively.

Nevertheless, despite the distinct superiority of ICA/DVA, the measurement noise of the voltage is unavoidably amplified when differentiating the voltage-capacity curve. Moreover, in order to obtain distinguishable peaks, the current rate adopted for ICA/DVA is generally restricted below a certain level, which may hinder its application in fast charging to some extent.

4.1.1.2. Temperature-based. Besides cell voltage, cell surface temperature is another auxiliary measurement monitored in BMS. When the lithium-ion battery is in operation, heat is generated or absorbed, causing a rise and drop in temperature. With the help of machine learning methods such as SVM (Klass et al., 2014; Yang et al., 2018a), ANN (Kim et al., 2019; Wu et al., 2016a), and GPR (Tagade et al., 2020; Yang et al., 2018c), accurate SOH estimation can be achieved even without the knowledge of battery internal reactions. Kim et al. (2019) used voltage and temperature to prove that it is possible to estimate SOH with reduced reference performance tests. The grouped measurements (voltage, current, and temperature in recent finite time) and the corresponding SOH values were regarded as the input of ANN. Tagade et al. (2020) proposed a deep GPR architecture, skipped the input feature extraction part, and directly used the partial charge-discharge time-series data for capacity estimation. The three dimensional data including voltage, temperature and time were selected randomly from a charging or discharging profile. The sequence length was 10 and the effectiveness of the algorithm was verified on aging datasets of batteries cycled at different C-rates, temperatures, and usage profiles. Li et al. (2014a) established the relationship between discharge capacity and multi-variable sample entropy (of temperature, charged capacity, and rest time), and then employed particle filter for SOH estimation.

By contrast, some researchers tend to focus on the principle behind a temperature change. The heat sources of the lithium-ion battery include Joule heat, reversible reaction heat, side reaction heat, and mixing heat. Eq. (9) shows the expression of temperature variation rate derived from the Joule heat and the reversible reaction heat which are the main heat sources to be considered in one cycle (Wu and Jossen, 2018). The temperature variation rate describes the entropic characteristic of the cell. Some possible explanations between temperature change and battery aging are given in (Tian et al., 2020b). Thus, the temperature change with time or voltage is a useful technique for SOH analysis. The temperature variation rate differentiates the temperature (T) with regard to the time (t) (i.e. dT/dt) while differential thermal voltammetry (DTV) differentiates the temperature (T) probed from the cell surface with respect to the terminal voltage (V) (i.e. dT/dV). The calculation of DTV is somehow similar to that of ICA, demonstrated in Eq. (10).

$$\begin{aligned} \frac{dT}{dt} &= \frac{\dot{Q}}{mc_p} - \frac{hA}{mc_p}(T - T_{env}) = \frac{\dot{Q}_{jou} + \dot{Q}_{re}}{mc_p} - \frac{hA}{mc_p}(T - T_{env}) \\ &= \frac{1}{mc_p}(I^2R + \frac{IT}{nF}\Delta S - hA(T - T_{env})) \end{aligned} \quad (9)$$

where \dot{Q} is the heat generation rate, \dot{Q}_{jou} is the Joule heat, \dot{Q}_{re} is the reversible reaction heat, ΔS is the entropy change, m is the cell mass, c_p is the cell heat capacity, h is the heat convection coefficient, A is the cell surface area, I is current, R is the charge or discharge resistance, n is the number of exchanged electrons, F is the Faraday constant, T is the cell temperature, and T_{env} is the environmental temperature.

$$DTV = \frac{dT}{dt} / \frac{dV}{dt} = \frac{dT}{dV} \quad (10)$$

where dT/dt is the differential of the temperature, dV/dt is the differential of the voltage.

The research team of Imperial College London employed DTV technique to track the battery aging mechanism (Shibagaki et al., 2018; Wu et al., 2015) and determine the SOH (Merla et al., 2016a, 2016b). They divided the sum of DTV into individual peaks, decoupling the different electrodes' effect, which corresponds to phases in the negative and positive electrode (Fig. 2). The peak parameters were used to quantitatively analyze the SOH. Wu and Jossen (2018) extracted the distance between two cooling areas from the temperature variation rate curve (dT/dt) during the CC charging process and used it for SOH estimation with maximum errors of +5.9% and -5.2%. Tian et al. (2020b) extracted the HI from the differential temperature curves calculated by the cell surface temperature during CC charging for SOH estimation. They claimed that, in combination with the conventional ICA-based method, the DTV-based method can improve the accuracy and robustness of the overall SOH estimation, while hardly increasing the computational burden.

Compared with the ICA, DTV provides complementary entropic information. Since the polarization effect is covered in the temperature change, it removes the need to be performed under a small current rate, making it promising for online applications. Only the measurements of terminal voltage and surface temperature are required, which means that they can be easily obtained via BMS and no extra apparatus is needed. Also, the isothermal condition is not a requirement for the DTV method, indicating that the heat dissipation condition is close to practice. Although the DTV method has advantages over the ICA, the same problem of ICA remains, that is, the effect of ambient temperature and C-rates on the DTV's features. Besides, it still faces the challenges of temperature measurement noise, surface thermal gradients, and machine-assisted feature interpretation. Finally, unlike the terminal voltage monitored by BMS, not all cells' temperatures are measured in the battery system, which somewhat limits the information available for pack SOH estimation.

4.1.1.3. Expansion-based. During the charging/discharging of the lithium-ion battery, the Li-ions are intercalated/de-intercalated into the negative electrode, and the electrode active material repeatedly expands and contracts. This phenomenon is found to be related to capacity fade, and the correlation between the strain/stress and capacity might be useful for SOH diagnosis (Mukhopadhyay and Sheldon, 2014). The expansion of the active material within the cell housing can lead to strains on the cell surface and, if constrained by additional casing structures (e.g. battery module casings), to forces outside the cell.

Dilatometry, strain and force are ways for investigation of material volume change (Popp et al., 2020). Oh et al. (2014) analyzed the correlation between the derivative of swelling related to the charge (ds/dQ) and the derivative of the potential over the charge (dV/dQ) under different C-rates utilizing cell dilation measurement. Schiffer et al. (2016) and Sommer et al. (2015) studied the first and second derivative

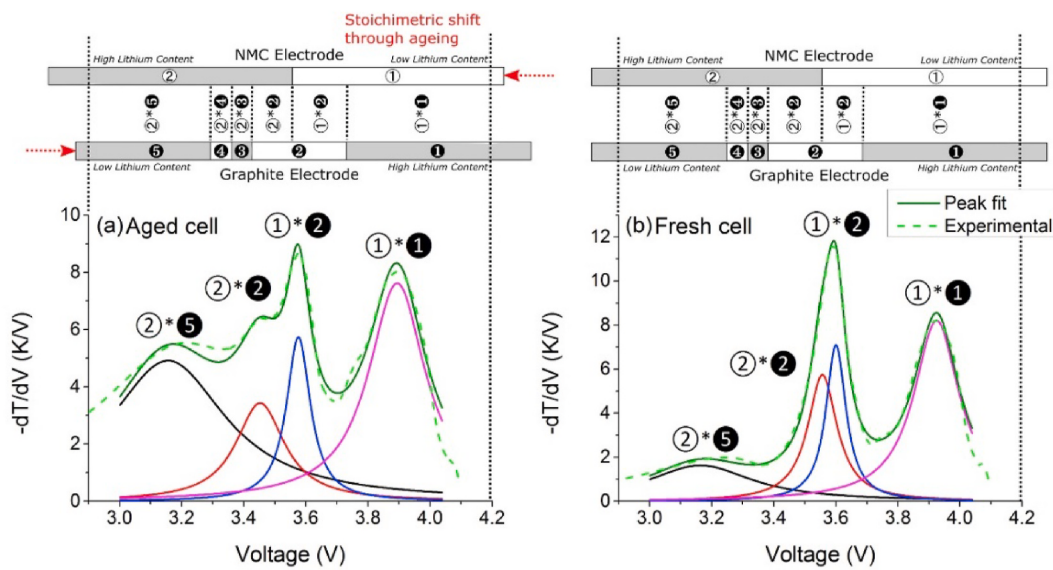


Fig. 2. Peak fitting of differential thermal voltammetry for (a) aged cell and (b) fresh cell. Adapted from (Merla et al., 2016b).

of strain to identify phase transitions with fiber optic sensors and dilatometer, respectively. (Cannarella and Arnold, 2014b) utilized the linear relationship between cell stress and SOH to estimate SOH and SOC which was believed to be associated with the SEI growth. The stack stress measurements were more sensitive to SOC than voltage, making it more convenient for SOC determination. As the stress can instantly respond to the lithium content in the electrodes, it can effectively detect the SOC difference caused by self-discharging compared with the conventional ampere-hour counting method. Samad et al. (2016) measured the force of $\text{Li}(\text{NiMnCo})\text{O}_2$ cells caused by the volume change of the electrodes during discharging to perform an ICA based on the mechanical signal. The peak position of the force-based IC curve was correlated with capacity fade and the proposed method achieved a maximum error of 3.1% for individual cell capacity estimation. The estimation methods of the references mentioned above mostly use the stress/strain of lithium-ion battery which is measured from outside rather than inside. Built-in fiber optic sensors may be a promising complementary tool for measuring internal strain (Ganguli et al., 2017; Raghavan et al., 2017) and temperature (David et al., 2009; Novais et al., 2016). The working principle of an optical fiber sensor is shown in Fig. 3. According to (Huang et al., 2020; Raijmakers et al., 2019), the fibre Bragg grating (FBG) sensor, which contains a periodic refractive index modification in the fiber core over a short distance, selectively reflects a short spectrum of the incident light depending on the magnitude of the effective refractive index and periodicity of the grating. The reflected spectrum is

used to monitor the physical perturbations to the FBG sensor (caused by temperature, pressure or strain). Ganguli et al. (2017) and Raghavan et al. (2017) fabricated large-format pouch cells with embedded fiber optic sensors to separate the temperature signal and the strain signal from the internal. The temperature was used as a compensation factor and the strain was utilized for SOC and capacity estimation. They showed that the strain was able to predict the capacity up to 10 cycles ahead for other cells with a maximum error of less than 2.2% based on the model built on one cell.

One of the most favorable aspects of using force instead of voltage in ICA is that the signal-to-noise ratio of force is much larger than that of voltage. However, the problem is that the external mechanical variation of cylindrical and prismatic cells may not be as obvious as that of pouch cells, and it demands a special apparatus for measurement. Additionally, as for the internal mechanical measurement, the impact of the built-in technique on battery operation or degradation still needs evaluation. Anyway, further investigations for the industrial application of mechanical-based methods have to be considered.

4.1.1.4. Ultrasound-based. Due to its non-destructive nature, ultrasonic inspection has proven to be effective in detecting internal defects (Mousavi et al., 2020; Sun and Zhu, 2020; Zeng et al., 2020), which in the case of the lithium-ion battery, are the delamination and ruffling of the electrode, the evolution of gas, and the degradation of material properties. The ultrasonic device can act as both an actuator and a

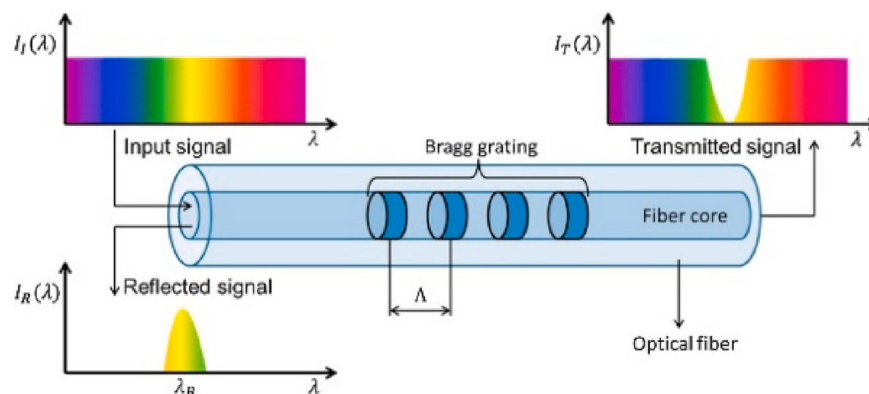


Fig. 3. Schematic of the operating principle of fibre Bragg grating sensor. Adapted from (Raijmakers et al., 2019).

sensor. By employing different modes of the transducers, through-body, reflection and surface measurement can be achieved. Fig. 4 shows the operating modes of these three ultrasound measurements on a pouch cell. The number 1, 2, 3 indicate the position of the ultrasonic sensor. The number 2 points at the position under the pouch cell, which is the mirrored position of number 1.

Sood et al. (2013) first proposed a health monitoring method using ultrasonic sensors. The sensors were set up to measure the reflection and transmission of the ultrasonic signals. They found that the 5 MHz ultrasonic pulse amplitude was significantly weakened for the aged cell. Hsieh et al. (2015) performed the reflection and through-body measurement using 2.25 MHz sampling frequency on pouch cells and cylindrical 18650 cells. They demonstrated the results of an acoustic time-of-flight (ToF) experiment of battery cycling and proposed a model to characterize SOC and SOH. The density distribution changes within the cells were probed and related to the acoustic signal amplitude and ToF. Wu et al. (2019) adopted the reflection measurement and investigated the evolution of the ultrasonic waves from a cycling test and an abusive test. The transducer was operated in a pulse-echo mode, where the ultrasonic signal was emitted and received by the same transducer with a pulse of 50 ns and a sampling frequency of 80 MHz. They found a strong dependence between the ToF and SOH and estimated the SOH using the ToF feature. An effective approach for the detection of early failure caused by overcharge is developed, which combines ultrasonic sensing and data fusion. Knehr et al. (2018) studied the full-cell cycling evolution of commercial lithium-ion batteries via ultrasonic through-body measurement. They found that the pressure within the cell would increase during the “break-in” period before the battery stabilized. The swelling of the graphite electrode was attributed to the decrease of the intrinsic moduli of the materials or the macroscopic changes in the electrode structure. Davies et al. (2017) conducted through-body ultrasonic testing on pouch cells. The ToF shift, the total signal amplitude of the high-frequency ultrasonic wave (2.25 MHz) were linked with the SOH using a machine learning model, achieving an average error of ~1%. Ladpli et al. (2018) discussed the feasibility of SOH estimation with ultrasonic guided surface waves. They applied the sine signal of a frequency of 125 kHz to pouch cells and found that the changes in ToF and signal amplitude resulting from shifts in the guided wave signals were strongly related to battery cycling and aging.

In general, these estimation methods based on the ultrasonic inspection are still at the early stages of exploration, especially for hard-case batteries. Despite its potential, the ultrasound waveform might be polluted by noise in practice, so validation on battery packs is necessary. Since the BMS is often not equipped with additional measurement devices other than voltage and temperature, the widespread adoption of these methods based on novel signals in practical application is hindered to some extent. However, these efforts are indispensable for a deeper understanding of the SOH evaluation of lithium-ion batteries.

4.1.2. Based on impedance

Battery degradation consists of thermodynamic fade and kinetics fade (Birk et al., 2017), where the latter is presented by the impedance increase along with battery aging (Chen et al., 2018b). Hence, some scholars also utilize impedance to describe battery SOH. The impedance will directly cause the voltage drop when the battery is operating, and therefore the reduction of power capability. Abundant approaches to the estimation of battery impedance have been developed, which can be roughly categorized into two types: time domain-based and frequency domain-based.

4.1.2.1. Time domain-based. In the time domain, one way to directly measure battery internal resistance is to use current pulses, with a time scale ranging from 10 ms to 10 s (Gao et al., 2018; Käbitz et al., 2013; Klass et al., 2014). Internal resistance comprises ohmic resistance and polarization resistance. The former has an instant effect on the voltage change while the latter takes some time to establish. Some researchers develop ECM to separate these two resistances with different time constants (Gao et al., 2016; Yang et al., 2018d). Based on a first-order ECM, the battery terminal voltage during discharge can be calculated as Eq. (11). The battery OCV can be regarded as invariant in a relatively short current pulse period, and the voltage difference during this period is therefore mainly attributed to the voltage drop caused by internal resistance. Thus, the battery resistance in different time scales can be roughly estimated by the voltage difference divided by the current difference. Käbitz et al. (2014) calculated the battery resistance using the 10s discharging voltage difference at 4C current rate from the specified pulse current test. The evolution of this 10s-resistance from the calendric and cyclic accelerated aging tests was analyzed.

$$U_t = U_{OCV}(SOC) - U_p - IR_0 \quad (11)$$

where the U_t is the measured terminal voltage, $U_{OCV}(SOC)$ is the OCV related to the SOC, U_p denotes the polarization voltage across the parallel RC circuit, R_0 is the ohmic resistance, and I is the applied current (positive for discharge).

Dai et al. (2009) proposed a SOH concept based on identifying ohmic resistance of a second-order ECM for power lithium-ion batteries. Dynamic profiles such as New European Drive Cycle (NEDC) (Chen et al., 2018b), Urban Dynamometer Driving Schedule (UDDS) (Chen et al., 2018b; Feng et al., 2015), Hybrid Pulse Power Characteristic (HPPC) (Xuan et al., 2020; Yang et al., 2018d) have been frequently employed to identify the resistance parameters derived from ECM which is used for SOH estimation and further state-of-power (SOP) prediction (Feng et al., 2015).

4.1.2.2. Frequency domain-based. In the frequency domain, battery internal resistance representing the electrochemical process can be determined using EIS, an effective non-destructive measurement technique to separate battery dynamic behavior. It measures the battery's

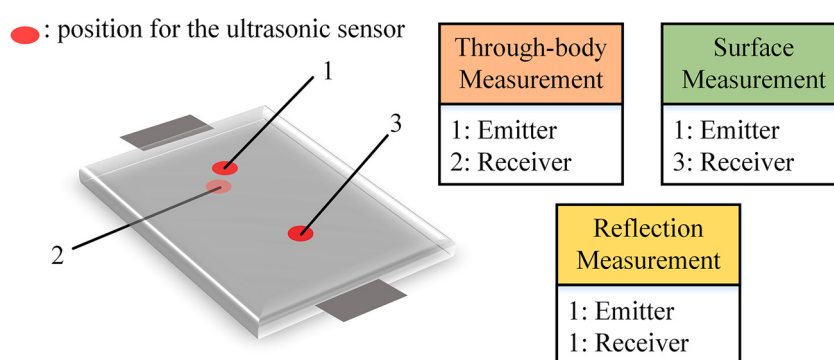


Fig. 4. Schematic of three measurement methods of ultrasonic sensing on a pouch cell.

response to a sine wave excitation over a wide spectrum of frequencies. The impedance is calculated by the ratio of excitation voltage to response current, which can be used as an indicator for battery SOH characterization. Fig. 5 illustrates a typical Nyquist plot of a battery obtained based on EIS. It contains three parts: a straight tail at low frequency, a large semi-circle at the middle frequency, and a small quarter-circle at high frequency (Li et al., 2014b). The low-frequency part correlates with the diffusion dynamics in the electrodes, the middle frequency part reflects the interfacial charge-transfer reaction together with the double layer capacitance effect, and the high-frequency part is associated with the SEI film and solid-phase contact resistance.

Eddahach et al. (2012) identified the parameters derived from an ECM containing five elements based on the testing results of EIS. The EIS was conducted at 25 °C with a frequency range of [0.01 Hz, 10 kHz]. Two parameters identified based on the measurement results of EIS were used to predict the RUL. Li et al. (2014b) did a similar test except that the 10 parameters to be identified were derived from an electrochemical impedance model. The EIS tests were carried out at two SOC levels (i.e. 100% and 50%), in the frequency range of [0.025Hz, 4 kHz]. Some parameters demonstrated the clear trend with battery aging, and the author claimed that model parameters of charge-transfer resistance and the SEI film resistance had the potential for SOH estimation.

Despite its superiority in identifying the degradation sources, EIS still requires high-accuracy equipment and a sophisticated test setup, which hinders its online application to some extent. Therefore, broadband signal design methods such as pulsed multisine and pseudo-random sequence have been proposed for battery impedance measurement and parameter identification (Fairweather et al., 2011; Sihvo et al., 2020a, 2020b). Pulsed multisine test attempts to simulate the real-world usage including the harmonic content for battery parameterization (Barai et al., 2019). Compared with the current pulse test, pulsed multisine test has been proven to improve the voltage model accuracy and greatly reduce the experimental time (Widanage et al., 2016a). Fig. 6 (a) demonstrates the designed signal of the pulsed multisine profile, which consists of a high current base signal and a relatively high-frequency multisine wave (Widanage et al., 2016b). It combines the advantages of the high current of pulse testing and the multi-frequency of EIS, and therefore has potential for online application of degradation analysis. Similarly, pseudo-random binary sequences have been proposed for onboard impedance diagnostics due to their simplicity of the signal generation (Fairweather et al., 2011; Geng et al., 2018; Yan et al., 2020). However, they are likely to reduce the measurement accuracy under battery nonlinearities. Thus, pseudo-random ternary sequences have been designed to suppress the effects of the second- and third-order nonlinearities (Sihvo et al., 2018, 2020a, 2020b). Fig. 6 (b) and (c) shows an example of the pseudo-random binary and ternary sequence in the time domain and frequency domain.

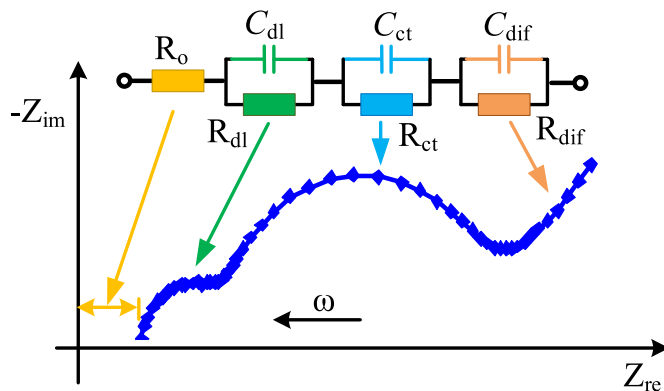


Fig. 5. A typical Nyquist plot obtained using electrochemical impedance spectrum.

To sum up, the time domain-based method is easy to implement for online estimation, but the separation of the dynamic process may not be so accurate. The frequency domain-based approach is more informative in splitting the impedance related to the electrochemical reaction process, but it requires a special measurement technique. A combination of current pulses and multisine sequences seems to be promising for a comprehensive description of battery dynamic degradation. The internal resistance value using the active current sequence is consistent with the measurement performed using EIS in the specific frequency range (Geng et al., 2018). The outcomes of internal resistance measured by the current step, alternating current injection, EIS and thermal loss are compared (Schweiger et al., 2010). It was concluded that a small pulse amplitude could lead to unacceptable large measurement uncertainties. In other words, a good signal to noise ratio needs to be reached. This is because the internal resistance of the battery is usually within the range of 0.1–20 mΩ. If a small pulse is applied, the voltage variation might not be distinguishable, which may induce large voltage measurement errors and lead to wrong conclusions. Therefore, it is suggested that the online SOH estimation methods based on impedance should carefully consider the time scale and the current amplitude under different application scenarios. Moreover, designing an active sequence of current pulses with various time scales is a future research trend for comprehensive SOH monitoring.

4.1.3. Based on aging mechanism parameters

As discussed in Section 3.1, the SOH should be defined in a broad sense to better monitor the changes from all possible aspects. Thus, the SOH defined by monitoring methods based on other aging mechanism parameters is also summarized here. These parameters are found to be sensitive to battery degradation, and we hope the summary would provide some guidance for the parameters to be considered in the SOH metric.

One way to obtain the aging-mechanism-based parameters is through the battery electrochemical model. Prasad and Rahn (2013) identified the parameters of a control-oriented single particle model. It was observed that the change of total resistance and change of solid-phase diffusion time in the positive electrode monotonically increased with battery aging. They defined two possible SOH calculation approaches, which are shown in Eqs. (12) and (13). Lyu et al. (2019) selected 7 out of 10 model parameters of a simplified electrochemical model as SOH indicators. Zhou et al. (2017) used a single particle model with the extended Kalman filter to estimate the number of cyclable Li-ions, which was considered as a health-relevant variable for monitoring. These indicators were derived from an electrochemical model using the voltage information.

$$SOH_{R_T^+}(t) = \frac{\hat{R}_T^+(t)}{\hat{R}_T^+(0)} \quad (12)$$

$$SOH_{\tau_D^+}(t) = \frac{\hat{\tau}_D^+(t)}{\hat{\tau}_D^+(0)} \quad (13)$$

where $\hat{R}_T^+(t)$ is the current cell resistance, $\hat{R}_T^+(0)$ is the initial cell resistance, $\hat{\tau}_D^+(t)$ is the present solid-phase diffusion time of Li⁺ species in the positive electrode, and $\hat{\tau}_D^+(0)$ is the initial solid-phase diffusion time of Li⁺ species in the positive electrode.

Another aging-mechanism-based parameter is the aging mode of the battery, which can quantitatively monitor SOH. Dubarry et al. (2012) presented a novel mechanistic model that can realize battery diagnosis and prognosis. The external voltage characteristics were explored via simulating the aging mode. From their point of view, battery capacity/resistance was insufficient in predicting the acceleration fading and providing an early warning due to the "silent" effect of loss of active material (Anseán et al., 2017). Therefore, they put forward a new indicator (the ratio of LAM_{NE} to the LLI) capable of recognizing the point

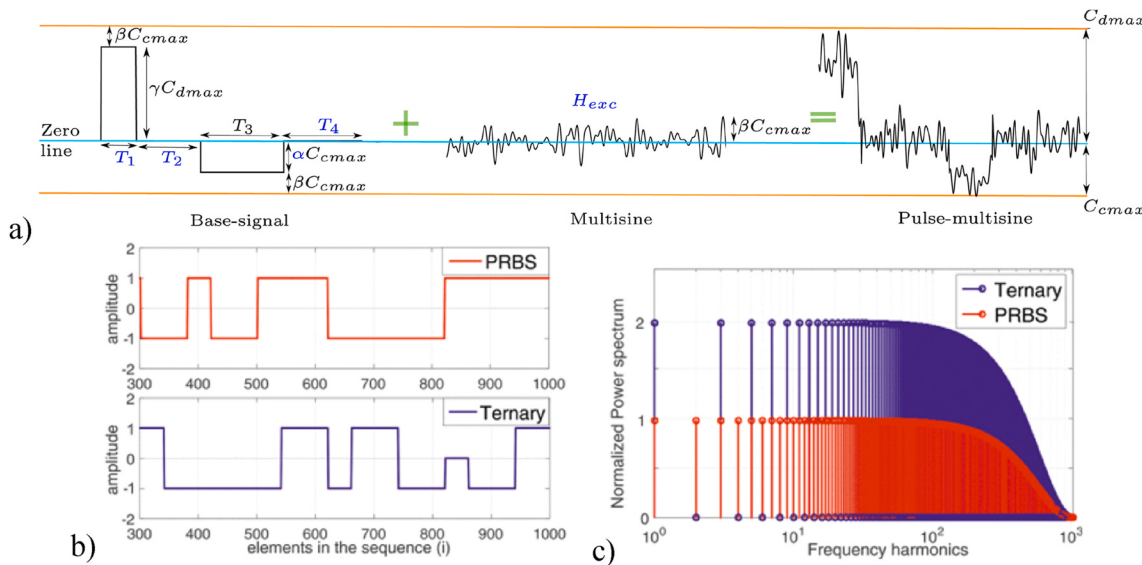


Fig. 6. (a) Design process of the pulsed multisine profile, adapted from (Widanage et al., 2016a, b); (b) characteristic of pseudo-random binary and ternary sequences in the time domain, and (c) power spectrums of pseudo-random binary and ternary sequences in the frequency domain. Adapted from (Sihvo et al., 2020b) (CC BY 4.0).

at which a silent degradation mode starts to contribute to a capacity loss (Baure and Dubarry, 2019; Dubarry et al., 2018). They concluded that the second stage of battery degradation (a nonlinear accelerated drop in capacity) would begin when the ratio (LAM_{NE}/LLI) is larger than 1. Mohtat et al. (2019) believed that the conventional SOH estimation based on capacity was not adequate for battery safety management since the limits may come from different electrodes along with the change of aging mode. Therefore, they introduced electrode-level state-of-health (eSOH) related parameters (individual electrode capacity and the utilization window) to reduce the risk of lithium plating based on monitoring the graphite lithiation state. They studied the identifiability of the parameters with and without cell expansion measurements and concluded that with the expansion measurement, the eSOH parameters could be estimated with a shallower DoD (less than 70%). They also analyzed the uncertainty of the electrode parameters estimation when the operation window was limited (Lee et al., 2018, 2020). However, the identification of either the aging modes or the electrode-related parameters still depends on the full-cell OCV, which means that the current rate needs to be relatively small to achieve a quasi-equilibrium state. Therefore, this method still needs studying for practical application under a high C-rate.

Apart from the aging-mechanism-based parameters mentioned above, the coulombic efficiency (CE), calculated by Eq. (14), has also been reported closely related to battery degradation (Li et al., 2019c). Yang et al. (2018c) investigated the long-term CE behaviors of two types of mainstream commercial lithium-ion batteries and suggested that the drastic decrease of the CE curve could be used for the inflection point warning of the accelerated aging. They found that the drop in the CE values may be induced by the loss of active material, and explained the relationship between the CE and aging rate from an electrochemical perspective. Burns et al. (2015) used high-precision CE measurement equipment to detect small amounts of lithium plating. They found that the onset of lithium plating would lead to the decrease of CE.

$$\eta = \frac{C_d}{C_c} \quad (14)$$

where C_d is the discharge capacity at a certain cycle, and C_c is the charge capacity in the same cycle.

Since one of the key functions of SOH monitoring is to ensure safe battery operation, here we also list some publications concerning lithium-plating detection. Lithium-plating or lithium deposition is

detrimental to battery safety, and it may lead to the internal short circuit of the battery, thereby triggering thermal runaway. It may occur when the charging rate of the battery exceeds the maximum intercalation rate of lithium-ions into the anode (Harlow et al., 2018). The deposition of lithium metal on the graphite clogs the pores, further reducing the intercalation rate, thereby promoting lithium deposition. This positive feedback would quickly lead to the nonlinear capacity drop and the sharp impedance increase. Petzl et al. (2015) found that the lithium plating that occurred at low temperature would affect the balance of the electrode and the inflection point exhibited on the capacity retention curve was responsive to the maximum aging rate of lithium plating. They also presented a lithium plating detection method based on high voltage plateau in the discharging profile and provided a quantitative estimation method using the DVA (Petzl and Danzer, 2014). Harlow et al. (2018) used the average charge-voltage and average discharge-voltage to identify the onset of lithium deposition. However, this method requires the same current rate of charging and discharging with a complete process. In addition, it assumes that the internal resistance of charging and discharging is the same and only LLI has occurred, which may not be valid on batteries undergoing different aging paths.

To put it in a nutshell, these aging-mechanism-based parameters or indicators used to characterize SOH are sensitive to the battery aging, but not all quantitative relationship is revealed in the literature. Unlike capacity or impedance, whose EOL thresholds are usually defined as 80% and 200% of the original values (Duong, 2000; Hu et al., 2019; Käbitz et al., 2013), the EOL thresholds for these novel parameters are still vacant, and extensive experiments are required for cross-validation. Moreover, although the aforementioned used SOH parameters were verified sufficiently, the feasibility and reliability of other battery types need further discussion. Last but not the least, a single characterization of SOH, either in terms of capacity or impedance, is not sufficient to comprehensively describe the battery aging and to grant the universality of the diagnostic method (Dubarry et al., 2020); therefore, there is an urgent need to develop a SOH estimation method that integrates multiple parameters.

4.2. For battery pack

The estimation methods of battery pack SOH can be divided into model-based methods and data-driven methods. The model-based method treats the whole pack or every single cell as an equivalent

circuit. For example, Bi et al. (2016) treated the entire battery pack as a whole and estimated the SOH based on the change of identified internal resistance derived from a second-order ECM. A new genetic resampling particle filter was proposed for SOH estimation to solve the problem of low accuracy of employed ECM. Although treating the whole pack as an equivalent circuit could greatly reduce the computational cost, more verification is required under larger cell-to-cell variation.

Hua et al. (2015) and Cordoba-arenas et al. (2015) estimated the pack SOH considering grouping and balancing approach. ECM was developed to model the cells' performance. The pack-level SOH was calculated through the cell-level SOH based on a multi time-scale estimation framework. Diao et al. (2017) quantitatively analyzed the relationship between the maximum available energy (MAE) of the pack and cell-to-cell variation. They found that both degradation and inconsistency of battery packs had a great impact on the maximum available energy of the battery system. Therefore, the MAE of the pack was considered as a HI and the MAE of a single cell is calculated based on a first-order ECM to obtain the MAE of the pack. Likewise, Zhang et al. (2018) also regarded the MAE as a HI, except that they defined the MAE using the OCV to SOC integration instead of the average OCV of entire SOC ranges. The battery pack was modeled by n first-order ECM in series. The particle swarm optimization-genetic algorithm and the recursive least square method were applied to identify the model parameters and update the cells' capacity respectively. However, the verification was conducted on a one-time dynamic working process and the influence of degradation was not taken into account. Wang et al. (2016) showed that the location interval between two inflection points on the DV curve can be used to represent cell SOH and a quantitative linear correlation between the transformation parameter of the DV and the cell nominal capacity was established. A pack SOH estimation framework was proposed for onboard monitoring. They claimed that the battery pack SOH could be evaluated based on the estimation results of all cells' capacities, but did not give a detailed description of the quantitative relationship. Jiang et al. (2019c) proposed a Copula-based battery pack consistency modeling method and applied it to the estimation of the battery pack energy utilization efficiency (EUE), which was considered as a HI. Unlike the pack SOH defined by the MAE or capacity mentioned above, EUE emphasizes the energy-delivery loss brought by the cell-to-cell variation in the battery pack (Jiang et al., 2019c). Its calculation is based on the single cell's parameters derived from a first-order ECM, which is shown in Eq. (15).

$$EUE = \frac{E_{\text{pack_dis}}}{E_{\text{pack_max}}} = \frac{\sum_{i=1}^N \int_{t_0}^{t_0 + \Delta t} (U_{\text{OCV},i}(t) \cdot I - R_i(t) \cdot I^2) dt}{\sum_{i=1}^N Q_i \cdot U_{\text{av}}} \quad (15)$$

where U_{av} represents the average OCV when the cell SOC changes from 100% to 0%, Q_i is the i th cell capacity, N is the number of series-connected cells, I is the applied current, $U_{\text{OCV},i}(t)$ and $R_i(t)$ are the OCV and internal resistance of the i th cell at a certain discharging time, and Δt is the time taken to discharge the pack.

Contrary to model-based methods, Song et al. (2020) estimated the battery pack capacity based on a feedforward neural network using the real-world datasets of EV and HEV. Accumulated mileage of vehicles, C-rates distribution during battery cycling, using intensity of SOC ranges, and distribution of cell temperatures were selected as input features of the ANN and the maximum relative error for pack capacity estimation was less than 4.5%. Love et al. (2014) proposed a single-point impedance (at 316 Hz) diagnostic method to monitor the SOH of single cells in packs of 4 cells series-connected. The overcharge abuse could be detected through the statistical $\mu \pm 3\sigma$ standard deviation threshold in the impedance response.

According to the literature summarized above, the current estimation methods of battery pack SOH still keep in a preliminary stage. The

major problem for the model-based methods is to strike a balance between the model accuracy and computational burdens. It is a promising research direction to estimate battery pack SOH by integrating cell SOH and inconsistency modeling. To be more specific, Fig. 7 demonstrates such a scheme for battery pack SOH estimation. It includes the degradation of a single cell and the deterioration of consistency, which are two aspects of pack aging. Therefore, two SOH definitions (SOH_{dif} and SOH_{max}) are employed when evaluating the pack SOH. Based on the multivariate distribution model of cells' inconsistency parameters, the reversible loss caused by the inconsistency of the pack can be calculated, and the MAE of the pack is obtained. As for the inconsistency modeling, Su et al. (2019) proposed a voltage compensation method to estimate the capacity imbalance in the battery pack. Song et al. (2019) conducted a numerical study on inconsistency analysis of series-connected lithium-ion battery pack via the charge cut-off voltage. Xu et al. (2020) estimated the relative SOH (i.e. the SOH differences of the series-connected cells) based on the wavelet analysis of the terminal voltage. These imbalance estimation methods are very important for battery pack SOH estimation and need to be further explored under different inconsistency levels.

5. The goals of lithium-ion battery SOH monitoring

Battery SOH serves as an indicator of the expected performance from the battery at the current state. Although numerous methods have been proposed for lithium-ion batteries health diagnostics and prognostics, the application scenarios they are oriented to are different, ranging from HEV to PV. The ultimate goals of battery SOH monitoring are to prolong the lifetime and enhance the reliability of the battery, which is proceeded by health management, involving system state estimation, battery optimal control, early warnings, etc. The function of SOH can be divided into two parts: short-term estimation and long-term prediction according to the published literature.

5.1. Short-term estimation

The short-term estimation consists of state determination and aging modes diagnosis. Other states like SOC, SOP, or state-of-energy (SOE) rely on the battery SOH more or less (Esfandyari et al., 2019). SOC, SOP and SOE represent the short-term capability of the battery which will vary along with degradation. Thus, these short-term states estimation methods usually need to consider the impact of SOH changes. SOH, or the capacity to be more specific, has been co-estimated with SOC (Chen et al., 2018a; Jiang et al., 2019a; Kim et al., 2013; Li et al., 2019b; Xiao et al., 2020). SOE and SOP estimation also need to consider the effect of battery capacity loss and impedance increase. Wang et al. (2013) exhibited a method for predicting the available power in a specific state of the battery (SOC, SOH and temperature), which was embodied in the used model parameters. Hu et al. (2018, 2020a) proposed a multi-scale co-estimation framework of SOC, SOH and SOP where the SOH was updated offline. The SOC and SOP were estimated in real-time based on the periodically updated parameters of a first-order ECM. Compared with SOC, it is more challenging to accurately estimate SOE because it not only involves capacity estimation but also needs to consider the nonlinear characteristic of the terminal voltage. Zhang et al. (2015) developed a model-based SOE and SOP joint estimation approach and thoroughly analyzed the robustness of the estimator against the uncertainty of temperature and degradation. Li et al. (2018) separated the fast and slow dynamics process in the electrical battery model and incorporated the effects of initial SOC, load C-rate, ambient temperature and SOH in the proposed model for robust SOE prediction.

In addition to state estimation, another function of SOH is to diagnose the aging mode, which is the key to battery safety operation. Herein, SOH is no longer limited to the battery capacity but includes more parameters to characterize the aging state of the battery, such as LAM_{PE} and LAM_{NE} . Pastor-Fernández et al. (2017) compared the IC-DV

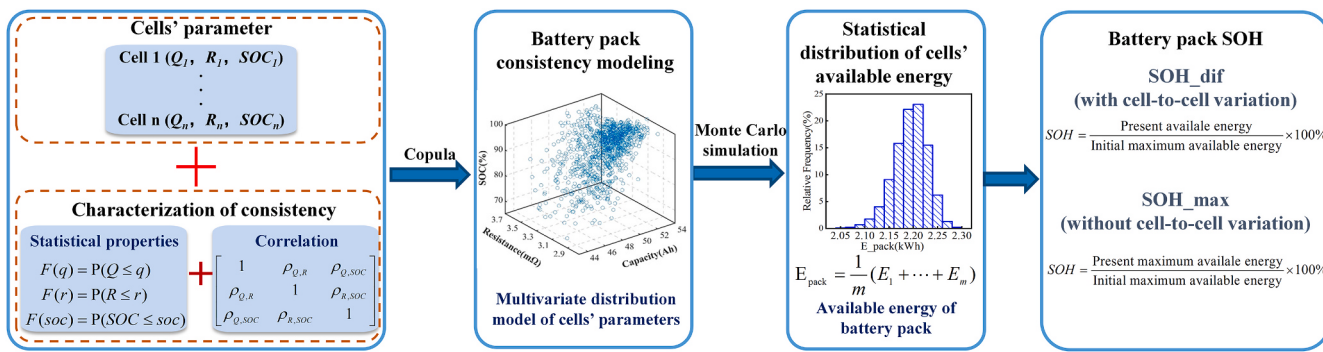


Fig. 7. A scheme for battery pack state-of-health estimation based on the present (maximum) available energy.

and EIS techniques to identify and quantify the effects of aging modes. The aging modes were quantitatively measured based on the features of the IC and OCV curves. Dubarry et al. (2012) presented a mechanistic approach to simulate battery aging modes via synthesizing the behaviors of two electrodes and discussed its application to battery diagnosis and prognosis. The essence of this approach was to fit the full-cell OCV by matching the electrode equilibrium potentials of the PE and the NE. It has been proven to be effective in the in-situ diagnosis of aging modes. In fact, it has been applied from LiFePO₄ (Han et al., 2014) to Li_xNi_{1/3}Mn_{1/3}Co_{1/3}O₂ and Li_xMn₂O₄ composite (Ma et al., 2018). Birk et al. (2017) further verified the algorithm on cells with LiCoO₂ and Li(NiCo)O₂ electrode for this in-situ quantitative diagnosis of degradation modes in lithium-ion batteries by testing coin cells with known material losses. This method focused on the analysis and diagnosis of the aging modes on a laboratory-level, and required a complete charging and discharging under a relatively small current rate to reach a quasi-equilibrium state. Marongiu et al. (2016) developed a method for onboard capacity estimation by means of half-cell curves. The approach collected the plateaus' lengths of LiFePO₄/graphite batteries to detect the aging modes. Dubarry et al. (2017) emulated the evolution of selected features of interest under the possible degradation paths and correlated the changes with the degradation diagnosis. Jiang et al. (2019b) directly used the OCV-capacity curves identified from the dynamic working profiles for synthesizing aging modes and compared the results of the non-real OCV-SOC curves with that of the real OCV-SOC. These methods mentioned above realize SOH diagnosis with partial SOC range and are promising in practice.

5.2. Long-term prediction

The long-term prediction chiefly refers to the multi-scale lifetime prognosis, including the first-life RUL and second-life accelerated fading recognition. For first-life evaluation, RUL is generally defined as the available cycling cycles or time when battery degraded to 70%–80% SOH (defined by capacity) (Duong, 2000; Ecker et al., 2012; Käbitz et al., 2013; Nuhic et al., 2013). Therefore, the RUL prediction problem is transformed into battery capacity estimation and its trend forecast. The result of RUL prediction serves as a decision-making indicator for the battery replacement ahead of a failure. The capacity estimation methods are elaborated in Section 4.1.1. We list some references for forecasting the capacity tendency in this sub-section.

Hu et al. (2020b) comprehensively summarized the battery lifetime prognostic techniques with a focus on model-based, data-driven, and hybrid methods. Fig. 8 sketches the main issues and focuses on current RUL prediction. The first part is to determine the parameters of either empirical model or data-driven model based on the historical data. In this process, measurement noise and capacity regeneration are the two main problems that need to be dealt with. The second part is to predict the RUL utilizing the model developed in the first part. One of the challenges in this part is that a sudden capacity drop may occur. To

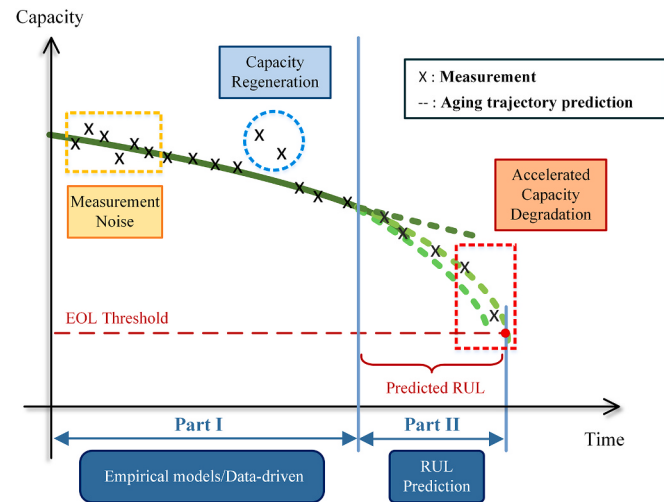


Fig. 8. Current issues and focuses on predicting battery remaining useful life.

tackle the problem of accelerated degradation before the EOL, Cong et al. (2020) improved the empirical degradation model and proposed an RUL prognostic method employing an unscented particle filter (UPF). It was claimed that the inflection point of the degradation was not the same as the sudden capacity drop point and it was more advanced in cycles. Even under the condition of the sudden capacity drop, the RUL estimation error was less than 0.52% compared with the conventional double exponential model. Kwon et al. (2020) carried out accelerated deterioration tests on LiNi_{0.5}Mn_{0.3}Co_{0.2}O₂ batteries and LiNi_{0.6}Mn_{0.2}Co_{0.2}O₂ batteries. The RUL was predicted with multiple linear regression and a recurrent neural network (RNN). The outcomes of different learning ratios were compared. The errors of proposed algorithms were within 5% (learning ratio larger than 85%) with accelerated aging of some batteries. Another challenge of RUL prediction is to evaluate the accuracy of the prognostic results. To meet this challenge, probabilistic algorithms such as Relevance Vector Machine (RVM) (Liu et al., 2015; Wang et al., 2013), GPR (Richardson et al., 2019; Yang et al., 2018a) have been developed. The algorithms for the prediction can be generally categorized into probabilistic and non-probabilistic. The former will give the probability density functions and confidence bounds of the prediction result, while the latter will only forecast an RUL value. The reader may refer to (Hu et al., 2020b; Li et al., 2019c) for more details, where several machine learning methods of RUL prognostics based on this classification were presented.

For second-life scenarios where an accelerated degradation may occur, SOH is a critical index for forecasting and evaluating long-term degradation. It often performs the function of assessing battery remaining value and identifying aging knee point. The degradation of secondary batteries is likely to accelerate (Johnen et al., 2021; Schuster

et al., 2015a; Yang et al., 2017). Plus, the performance of single-cell tends to differ in a pack due to inhomogeneous temperature and current distributions (Jiang et al., 2017; Schuster et al., 2015b). With larger cell-to-cell variations and the risk of performance plunging, predicting the RUL for echelon batteries is even more challenging. Diao et al. (2019a) defined the knee point as the cycle number at the intersection of two tangent lines on the capacity fade curves and developed an algorithm to detect it. However, this method still requires a great deal of data after acceleration. Zhang et al. (2019) put forward an acceleration knee point recognition method incorporated with quantile regression and Monte Carlo simulation. The proposed method was able to recognize the knee point effectively even when the input was disturbed and it was expected to provide an early warning before battery failure. These methods mostly emphasize the identification algorithms from the data angle, while the role of changes in aging mechanism in recognizing the knee point has been underestimated. Sarasketa-Zabala et al. (2015) evaluated the accelerated aging mechanism of cycling lithium-ion batteries through in-situ and ex-situ analysis, with the dominant aging mechanism of SEI layer growth in the primary stage and localized lithium plating on the negative electrode in the acceleration stage. Gao et al. (2019) conducted cycle life tests under various external conditions until capacity degradation accelerated. The evolution characteristics of battery aging modes along with cycling were identified through an improved non-destructive diagnostic algorithm and the mechanisms of acceleration were analyzed. Schuster et al. (2015a) observed a turning point from linear to nonlinear degradation and analyzed the dependency of this nonlinear aging characteristics on the voltage change, C-rate, and temperature. The dominating aging mechanism was investigated via EIS and SEM techniques. However, few studies have applied aging mechanism analysis to the identification of battery accelerated degradation. Therefore, it is urgent and necessary for developing an accelerated fading identification algorithm to be integrated with the aging mechanisms.

6. Challenges and prospects

Significant improvement has been made in the techniques of SOH diagnostics and prognostics over the last decade. However, the current research on the description of SOH is still insufficient and still faces several problems, especially for its application to health and safety management, which is still in the relatively early stage. The challenges and prospects are summarized from the perspective of SOH characterization, estimation and application.

6.1. Problems and challenges

There are still some major challenges relating to the comprehensive description of SOH, its estimation and application:

- (1) The internal state of the battery cannot be directly measured. And it is also difficult to monitor and model through the external behaviors since the external behaviors are a combination of multiple internal reactions which are usually coupled with each other.
- (2) Battery aging mechanisms have not been fully understood yet. For instance, it is believed that the growth of the SEI layer is the main aging cause under mild aging condition (C-rate@1C, T@25 °C). However, "abnormal" phenomenon such as sudden capacity drop has been observed even under mild aging condition (Gao et al., 2019), which indicates an aging mechanism different from SEI growth.
- (3) The diversity of aging paths challenges SOH estimation and prediction. Different aging conditions could present the same capacity/resistance at a certain stage and vary significantly in the following stage, which confirms the necessity to develop a multi-parameters SOH metric.

- (4) The common measurements of BMS include voltage, current, and temperature, which are manifestations of the interplay of several internal electrochemical processes. The extraction and estimation of appropriate parameters to comprehensively characterize SOH based on the available working data remain a challenge.
- (5) Unlike capacity or impedance, which has an explicit EOL threshold, the EOL threshold for the aging-mechanism-based parameters is still vacant, and extensive experiments are required for cross-validation.
- (6) The mapping relationship of SOH from the individual cell to the battery pack is not distinct. The gap in the scale of the number of cells, module/pack structure design between laboratory and industry challenges the accuracy and feasibility of the pack SOH monitoring in practical application.
- (7) Another problem is to strike a balance between the model complexity and computational burdens for pack SOH estimation. Although the SOH does not necessarily need to be updated instantly like SOC due to its slow varying characteristics, it does not mean that the computational cost is low. This is because the pack SOH closely relies on the state of each cell and the number of single cells in the pack/system level is considerable.
- (8) The validation of the proposed SOH estimation methods is insufficient. Most of them are verified on cells cycling under constant current with fixed ambient temperature (Berecibar et al., 2016a; Bian et al., 2019; Tian et al., 2020b). Very few aging tests are carried out under dynamics driving profiles (Baure and Dubarry, 2019; You et al., 2016), let alone the pack SOH diagnostics with different levels of inconsistency.

6.2. Prospects for future development

Based on the previous sub-sections, there is still a wide gap between SOH research and industrial implementation. To better conduct future studies, we discuss some critical tasks and potential research directions from the following three aspects, outlined in Fig. 9.

(1) SOH characterization

To comprehensively characterize battery SOH, detailed aging mechanism studies at different levels are necessary. Most of the degradation tests are single-stress-factor-based and are performed at cell-level, which is not conducive for an in-depth understanding of the battery system degradation with inconsistency. Therefore, aging tests at the cell level which include coupling stress factors such as variant current and variant temperature need to be conducted. Aging tests at pack-level may be a beneficial investigation method for analyzing the evolution of inconsistency throughout the pack degradation.

For SOH metric construction studies, it is recommended that the selection of the specific parameters or indicators should be function-oriented. There is usually a great deal of aging-sensitive parameters in the SOH model, and these parameters should play a decision-making role for reliable and safe operation. Many pieces of literature have ignored the important role of the SOH parameters in the later stage of health management, leading to the gap between battery SOH estimation and SOH application. The lithiation state of graphite or the potential of graphite is one of the key parameters in battery optimization charging since it is closely related to lithium plating (Tomaszewska et al., 2019). Unfortunately, most of the SOH estimation approaches still focus on the SOH defined by capacity or resistance, and there is little discussion of relevant SOH monitoring method for graphite potential, which should be considered as one parameter in the SOH metric. The traditional SOH definitions and functions have weaken the guiding significance of the battery degradation mechanism for prognostic health management. And future investigation on aging-mechanism-based parameters for SOH estimation needs to be conducted.

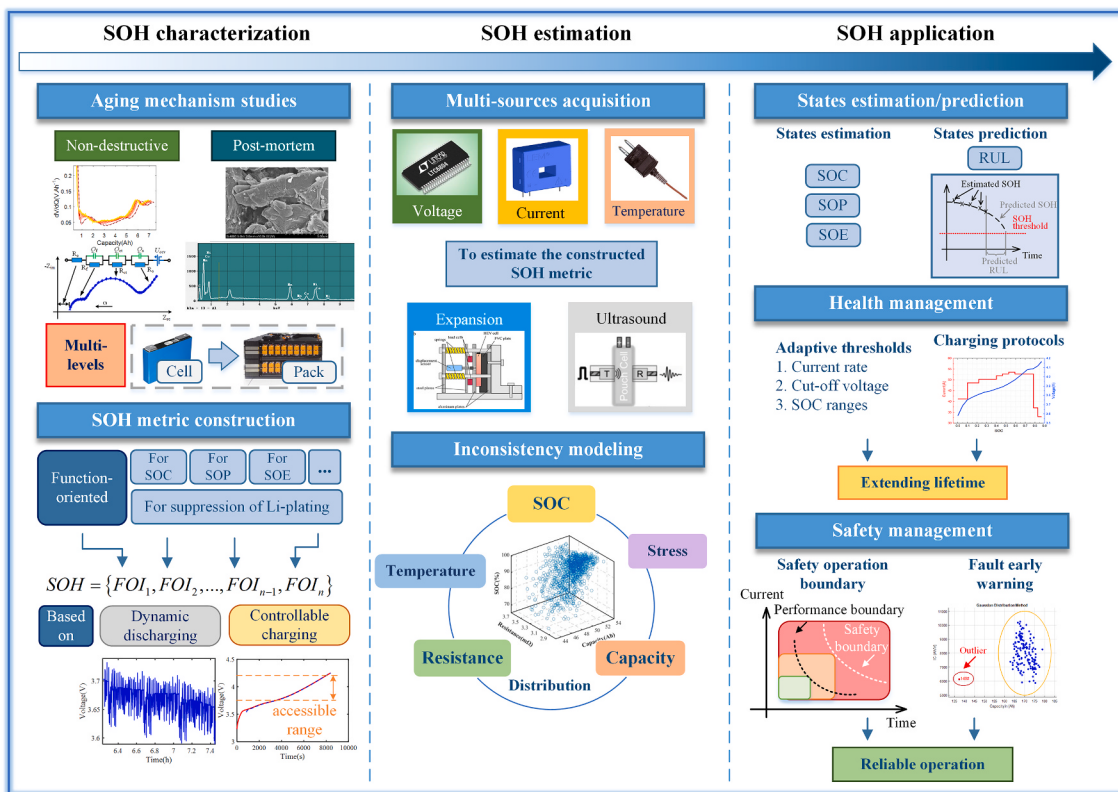


Fig. 9. Prospects of state-of-health characterization, estimation and application for lithium-ion batteries. Figures of expansion and ultrasound adapted from (Knehr et al., 2018; Sauerteig et al., 2018).

(2) SOH estimation

Firstly, a trade-off between model complexity and computational efficiency needs to be made. Due to its remarkable benefits of probing battery internal aging mechanisms, the implementation of the electrochemical model is becoming an inevitable trend in battery health management. The high precision of the complexity model comes along with the high computational cost. Fortunately, with the development of 5G technology and cloud BMS (Kim et al., 2018; Li et al., 2019a; Li et al., 2020), data collection and storage problems together with the limited computing resources have been alleviated to some extent. Therefore, further study concerning developing a hybrid method that combines aging mechanism model and machine learning algorithms based on the framework of cloud BMS for SOH monitoring and forecasting might be a promising direction.

Secondly, the extraction and estimation of the SOH feature under dynamic discharging and controllable charging process is an urgent and necessary task. The situation is rare where batteries can be fully exhausted or fully charged in a pack level in practice, therefore, the SOH estimation method should take the battery operation range into account. Besides, the quality of the practical data is not as accurate as that of the laboratory whose voltage sampling frequency can reach 100 Hz with a measurement error of ± 0.1 mV. It is quite necessary to conduct further research from the perspective of the effect of data quality and quantity on SOH diagnosis or prognosis.

Thirdly, inconsistency modeling is a notable aspect of pack SOH estimation. Most of the current SOH monitoring methods have been conducted and verified at the cell level. Nevertheless, in the practical applications of a battery-powered system, large-scale lithium-ion battery packs are equipped, which are composed of multiple individual cells connected in series and/or parallel to meet energy or power requirements. Temperature gradient (Klein et al., 2016; Paul et al., 2013), current non-uniformity (Pastor-Fernández et al., 2017), manufacturing

variances (Baumhöfer et al., 2014), and other factors can lead to the inconsistency in cell performance, resulting in a deterioration of pack performance. Therefore, the imbalance modeling comprising the description of consistency dependence among battery parameters needs continuous research.

Finally, with the development of sensor integration technology such as fiber optic sensors (Ganguli et al., 2017; Raghavan et al., 2017; Sommer et al., 2015) or built-in piezoelectric sensors (Ladpli et al., 2018), it is attractive to employ different sensors for comprehensive monitoring. SOH estimation with fusing multi-signals is likely to become a research hotspot in the future.

(3) SOH application

In general, there is still a wide gap between SOH diagnostics and SOH application. “How to use the diagnostic result in further health management” is not fully discussed in most published research. Based on the goals of SOH monitoring, we believe that the function of SOH prognosis is more than just a pure judgment of battery retirement point but instructive guidance of battery aging process, which includes performance optimization and safety management. Woody et al. (2020) investigated the recommendations from the manufacturers to preserve battery health and presented some suggestions for the battery lifetime extension from the user side. However, the provided nine practices are quite general and more detailed health management strategies from the developer-side still need to be explored. More specifically, the charging cut-off conditions and charging C-rate should be adaptive along with aging state to extend battery lifetime. Safety operation boundary should also be further investigated for early warning. In fact, relevant research on SOH indicators or parameters used to formulate battery health management strategies is still in its infancy, and we think this is a promising aspect for future research.

7. Conclusions

This paper systematically overviews the SOH research status of lithium-ion batteries from the perspective of characterizations, estimations and applications. SOH definition that is limited to battery capacity or impedance estimation is not conducive to comprehensively characterizing the aging state of the battery. Therefore, it should be defined in a broad sense. Establishing a multi-parameters SOH metric with internal aging mechanism changes included is recommended. Apart from the cell-level SOH definition, a focus on pack-level SOH is also developed. It is suggested that the definition of pack-level SOH should comprehensively consider the cell-to-cell variations and the ability to deliver energy.

Cell-level SOH estimation methods are categorized by the type of parameters used for SOH characterization. None of the diagnostic methods reviewed is a universal solution; instead, an inherent balance between model complexity and model accuracy needs to be investigated. Fortunately, with the advent of cloud BMS with 5G technologies and built-in integrated sensors with multiple signals, an electrochemical-mechanical-thermal coupled model combining machine learning approaches might be possible for remote SOH monitoring. When selecting the SOH metric for diagnosis and employing the algorithms for prognosis, both the researchers and the technologists are encouraged to consider the battery external operation conditions, the internal degradation modes, the goals of selected SOH-related parameters, and data accessibility.

Currently, there is still a wide gap between SOH estimation and application. The present SOH prognostic methods mainly include short-term state estimation and long-term RUL prediction, which is only a pure judgment of battery retirement point and neglects the instructive significance of the battery aging process in health management. How to use the diagnostic results for extending battery life and ensuring safe operation is a highlighted open issues. Relevant research on SOH indicators or parameters used to formulate battery health management strategies needs to be carried out in the future.

Declaration of competing interest

The authors declare that they have no known competing financial interests or personal relationships that could have appeared to influence the work reported in this paper.

Acknowledgements

This work was supported by the National Natural Science Foundation of China (Grant No. 51977007, Grant No. 61633015, Grant No. 52007006). The authors would like to thank Dr. Yan Jiang, Dr. Haijun Ruan and Xitian He for providing relevant data and their insightful discussion. The authors are also grateful to the editors and the reviewers for their constructive comments that contributed to improving the paper.

References

- Anseán, D., Dubarry, M., Devie, A., Liaw, B.Y., García, V.M., Viera, J.C., González, M., 2017. Operando lithium plating quantification and early detection of a commercial LiFePO₄ cell cycled under dynamic driving schedule. *J. Power Sources* 356, 36–46. <https://doi.org/10.1016/j.jpowsour.2017.04.072>.
- Anseán, D., García, V.M., Gonzalez, M., Blanco-Viejo, C., Viera, J.C., Pulido, Y.F., Sanchez, L., 2019. Lithium-ion battery degradation indicators via incremental capacity analysis. *IEEE Trans. Ind. Appl.* 55, 2992–3002. <https://doi.org/10.1109/TIA.2019.2891213>.
- Burai, A., Tangirala, R., Uddin, K., Chevalier, J., Guo, Y., McGordon, A., Jennings, P., 2017. The effect of external compressive loads on the cycle lifetime of lithium-ion pouch cells. *J. Energy Storage* 13, 211–219. <https://doi.org/10.1016/j.est.2017.07.021>.
- Burai, A., Uddin, K., Dubarry, M., Somerville, L., McGordon, A., Jennings, P., Bloom, I., 2019. A comparison of methodologies for the non-invasive characterisation of commercial Li-ion cells. *Prog. Energy Combust. Sci.* 72, 1–31. <https://doi.org/10.1016/j.pecs.2019.01.001>.
- Baumhöfer, T., Brühl, M., Rothgang, S., Uwe, D., 2014. Production caused variation in capacity aging trend and correlation to initial cell performance. *J. Power Sources* 247, 332–338. <https://doi.org/10.1016/j.jpowsour.2013.08.108>.
- Baure, G., Dubarry, M., 2019. Synthetic vs. Real driving cycles: a comparison of electric vehicle battery degradation. *Batteries* 5, 42. <https://doi.org/10.3390/batteries5020042>.
- Benavente-Araoz, F., Varini, M., Lundblad, A., Cabrera, S., Lindbergh, G., 2020. Effect of partial cycling of NCA/graphite cylindrical cells in different SOC intervals. *J. Electrochem. Soc.* 167, 040529. <https://doi.org/10.1149/1945-7111/ab78fd>.
- Berecibar, M., Devriendt, F., Dubarry, M., Villarreal, I., Omar, N., Verbeke, W., Van Mierlo, J., 2016a. Online state of health estimation on NMC cells based on predictive analytics. *J. Power Sources* 320, 239–250. <https://doi.org/10.1016/j.jpowsour.2016.04.109>.
- Berecibar, M., Gandiaga, I., Villarreal, I., Omar, N., Van Mierlo, J., Van den Bossche, P., 2016b. Critical review of state of health estimation methods of Li-ion batteries for real applications. *Renew. Sustain. Energy Rev.* 56, 572–587. <https://doi.org/10.1016/j.rser.2015.11.042>.
- Bi, J., Zhang, T., Yu, H., Kang, Y., 2016. State-of-health estimation of lithium-ion battery packs in electric vehicles based on genetic resampling particle filter. *Appl. Energy* 182, 558–568. <https://doi.org/10.1016/j.apenergy.2016.08.138>.
- Bian, X., Liu, L., Yan, J., 2019. A model for state-of-health estimation of lithium ion batteries based on charging profiles. *Energy* 177, 57–65. <https://doi.org/10.1016/j.energy.2019.04.070>.
- Bian, X., Liu, L., Yan, J., Zou, Z., Zhao, R., 2020. An open circuit voltage-based model for state-of-health estimation of lithium-ion batteries: model development and validation. *J. Power Sources* 448. <https://doi.org/10.1016/j.jpowsour.2019.227401>.
- Birkl, C.R., Roberts, M.R., McTurk, E., Bruce, P.G., Howey, D.A., 2017. Degradation diagnostics for lithium ion cells. *J. Power Sources* 341, 373–386. <https://doi.org/10.1016/j.jpowsour.2016.12.011>.
- Bodenes, L., Naturel, R., Martinez, H., Dedryvère, R., Menetrier, M., Croguennec, L., Péres, J., Tessier, C., Fischer, F., 2013. Lithium secondary batteries working at very high temperature : capacity fade and understanding of aging mechanisms. *J. Power Sources* 236, 265–275. <https://doi.org/10.1016/j.jpowsour.2013.02.067>.
- Burns, J.C., Stevens, D.A., Dahn, J.R., 2015. In-situ detection of lithium plating using high precision coulometry. *J. Electrochem. Soc.* 162, A959–A964. <https://doi.org/10.1149/2.0621506jes>.
- Cannarella, J., Arnold, C.B., 2014a. Stress evolution and capacity fade in constrained lithium-ion pouch cells. *J. Power Sources* 245, 745–751. <https://doi.org/10.1016/j.jpowsour.2013.06.165>.
- Cannarella, J., Arnold, C.B., 2014b. State of health and charge measurements in lithium-ion batteries using mechanical stress. *J. Power Sources* 269, 7–14. <https://doi.org/10.1016/j.jpowsour.2014.07.003>.
- Chen, C., Xiong, R., Shen, W., 2018a. A lithium-ion battery-in-the-loop approach to test and validate multiscale dual H infinity filters for state-of-charge and capacity estimation. *IEEE Trans. Power Electron.* 33, 332–342. <https://doi.org/10.1109/TPEL.2017.2670081>.
- Chen, L., Lü, Z., Lin, W., Li, J., Pan, H., 2018b. A new state-of-health estimation method for lithium-ion batteries through the intrinsic relationship between ohmic internal resistance and capacity. *Measurement* 116, 586–595. <https://doi.org/10.1016/j.measurement.2017.11.016>.
- Cong, X., Zhang, C., Jiang, J., Zhang, W., Jiang, Y., Jia, X., 2020. An improved unscented particle filter method for remaining useful life prognostic of lithium-ion batteries with Li(NiMnCo)O₂ cathode with capacity diving. *IEEE Access* 8, 58717–58729. <https://doi.org/10.1109/ACCESS.2020.2978245>.
- Cordoba-arenas, A., Onori, S., Rizzoni, G., 2015. A control-oriented lithium-ion battery pack model for plug-in hybrid electric vehicle cycle-life studies and system design with consideration of health management. *J. Power Sources* 279, 791–808. <https://doi.org/10.1016/j.jpowsour.2014.12.048>.
- Dai, H., Wei, X., Sun, Z., 2009. A new SOH prediction concept for the power lithium-ion battery used on HEVs. In: 5th IEEE Vehicle Power and Propulsion Conference (VPPC 09). IEEE Vehicle Power and Propulsion Conference, pp. 1649–1653.
- David, N.A., Wild, P.M., Hu, J., Djilali, N., 2009. In-fibre Bragg grating sensors for distributed temperature measurement in a polymer electrolyte membrane fuel cell. *J. Power Sources* 192, 376–380. <https://doi.org/10.1016/j.jpowsour.2009.03.021>.
- Davies, G., Knehr, K.W., Van Tassell, B., Hodson, T., Biswas, S., Hsieh, A.G., Steinart, D. A., 2017. State of charge and state of health estimation using electrochemical acoustic time of flight analysis. *J. Electrochem. Soc.* 164, A2746–A2755. <https://doi.org/10.1149/2.1411712jes>.
- de Hoog, J., Timmermans, J.M., Ioan-Stroe, D., Swierczynski, M., Jaguemont, J., Goutam, S., Omar, N., Van Mierlo, J., Van Den Bossche, P., 2017. Combined cycling and calendar capacity fade modeling of a Nickel-Manganese-Cobalt Oxide Cell with real-life profile validation. *Appl. Energy* 200, 47–61. <https://doi.org/10.1016/j.apenergy.2017.05.018>.
- Diao, W., Jiang, J., Zhang, C., Liang, H., Pecht, M., 2017. Energy state of health estimation for battery packs based on the degradation and inconsistency. In: Energy Procedia. Elsevier B.V., pp. 3578–3583. <https://doi.org/10.1016/j.egypro.2017.12.248>.
- Diao, W., Naqvi, I.H., Pecht, M., 2020. Early detection of anomalous degradation behavior in lithium-ion batteries. *J. Energy Storage* 32, 101710. <https://doi.org/10.1016/j.est.2020.101710>.
- Diao, W., Saxena, S., Han, B., Pecht, M., 2019a. Algorithm to determine the knee point on capacity fade curves of lithium-ion cells. *Energies* 12, 2910. <https://doi.org/10.3390/en12152910>.

- Diao, W., Saxena, S., Pecht, M., 2019b. Accelerated cycle life testing and capacity degradation modeling of LiCoO₂-graphite cells. *J. Power Sources* 435. <https://doi.org/10.1016/j.jpowsour.2019.226830>.
- Dubarry, M., Baure, G., Anseán, D., 2020. Perspective on state-of-health determination in lithium-ion batteries. *J. Electrochem. Energy Convers. Storage* 17, 1–8. <https://doi.org/10.1115/1.4045008>.
- Dubarry, M., Baure, G., Devie, A., 2018. Durability and reliability of EV batteries under electric utility grid operations: path dependence of battery degradation. *J. Electrochim. Soc.* 165, A773–A783. <https://doi.org/10.1149/2.0421805jes>.
- Dubarry, M., Berecibar, M., Devie, A., Anseán, D., Omar, N., Villarreal, I., 2017. State of health battery estimator enabling degradation diagnosis: model and algorithm description. *J. Power Sources* 360, 59–69. <https://doi.org/10.1016/j.jpowsour.2017.05.121>.
- Dubarry, M., Truchot, C., Liaw, B.Y., 2012. Synthesize battery degradation modes via a diagnostic and prognostic model. *J. Power Sources* 219, 204–216. <https://doi.org/10.1016/j.jpowsour.2012.07.016>.
- Duong, T.Q., 2000. USABC and PNGV test procedures. *J. Power Sources* 244–248.
- Ecker, M., Gerschler, J.B., Vogel, J., Käbitz, S., Hust, F., Dechent, P., Sauer, D.U., 2012. Development of a lifetime prediction model for lithium-ion batteries based on extended accelerated aging test data. *J. Power Sources* 215, 248–257. <https://doi.org/10.1016/j.jpowsour.2012.05.012>.
- Ecker, M., Nieto, N., Käbitz, S., Schmalstieg, J., Blanke, H., Warnecke, A., Sauer, D.U., 2014. Calendar and cycle life study of Li(NiMnCo)O₂-based 18650 lithium-ion batteries. *J. Power Sources* 248, 839–851. <https://doi.org/10.1016/j.jpowsour.2013.09.143>.
- Eddahach, A., Briat, O., Bertrand, N., Delétage, J.Y., Vinassa, J.M., 2012. Behavior and state-of-health monitoring of Li-ion batteries using impedance spectroscopy and recurrent neural networks. *Int. J. Electr. Power Energy Syst.* 42, 487–494. <https://doi.org/10.1016/j.ijepes.2012.04.050>.
- Esfandyari, M.J., Esfahanian, V., Hairi Yazdi, M.R., Nehzati, H., Shekoofa, O., 2019. A new approach to consider the influence of aging state on Lithium-ion battery state of power estimation for hybrid electric vehicle. *Energy* 176, 505–520. <https://doi.org/10.1016/j.energy.2019.03.176>.
- Fairweather, A.J., Foster, M.P., Stone, D.A., 2011. Battery parameter identification with pseudo random binary sequence excitation (PRBS). *J. Power Sources* 196, 9398–9406. <https://doi.org/10.1016/j.jpowsour.2011.06.072>.
- Farmann, A., Waag, W., Marongiu, A., Sauer, D.U., 2015. Critical review of on-board capacity estimation techniques for lithium-ion batteries in electric and hybrid electric vehicles. *J. Power Sources* 281, 114–130. <https://doi.org/10.1016/j.jpowsour.2015.01.129>.
- Feng, T., Yang, L., Zhao, X., Zhang, H., Qiang, J., 2015. Online identification of lithium-ion battery parameters based on an improved equivalent-circuit model and its implementation on battery state-of-power prediction. *J. Power Sources* 281, 192–203. <https://doi.org/10.1016/j.jpowsour.2015.01.154>.
- Feng, X., Pan, Y., He, X., Wang, L., Ouyang, M., 2018. Detecting the internal short circuit in large-format lithium-ion battery using model-based fault-diagnosis algorithm. *J. Energy Storage* 18, 26–39. <https://doi.org/10.1016/j.est.2018.04.020>.
- Ganguli, A., Saha, B., Raghavan, A., Kiesel, P., Arakaki, K., Schuh, A., Schwartz, J., Hegyi, A., Sommer, L.W., Lochbaum, A., Sahu, S., Alamgir, M., 2017. Embedded fiber-optic sensing for accurate internal monitoring of cell state in advanced battery management systems part 2: internal cell signals and utility for state estimation. *J. Power Sources* 341, 474–482. <https://doi.org/10.1016/j.jpowsour.2016.11.103>.
- Gao, W., Zou, Y., Sun, F., Hu, X., Yu, Y., Feng, S., 2016. Data pieces-based parameter identification for lithium-ion battery. *J. Power Sources* 328, 174–184. <https://doi.org/10.1016/j.jpowsour.2016.08.018>.
- Gao, Y., Jiang, J., Zhang, C., Zhang, W., Jiang, Y., 2018. Aging mechanisms under different state-of-charge ranges and the multi-indicators system of state-of-health for lithium-ion battery with Li(NiMnCo)O₂ cathode. *J. Power Sources* 400, 641–651. <https://doi.org/10.1016/j.jpowsour.2018.07.018>.
- Gao, Y., Yang, S., Jiang, J., Zhang, C., Zhang, W., Zhou, X., 2019. The mechanism and characterization of accelerated capacity deterioration for lithium-ion battery with Li(NiMnCo)O₂ cathode. *J. Electrochim. Soc.* 166, A1623–A1635. <https://doi.org/10.1149/2.1001908jes>.
- Geng, Z., Thiringer, T., Olofsson, Y., Groot, J., West, M., 2018. On-board impedance diagnostics method of Li-ion traction batteries using pseudo-random binary sequences. 2018 20th Eur. Conf. Power Electron. Appl. EPE 2018 ECCE Eur. 1–10.
- Guau, T., Zuo, P., Sun, S., Du, C., Zhang, L., Cui, Y., Yang, L., Gao, Y., Yin, G., Wang, F., 2014. Degradation mechanism of LiCoO₂/mesocarbon microbeads battery based on accelerated aging tests. *J. Power Sources* 268, 816–823. <https://doi.org/10.1016/j.jpowsour.2014.06.113>.
- Guo, Z., Qiu, X., Hou, G., Liaw, B.Y., Zhang, C., 2014. State of health estimation for lithium ion batteries based on charging curves. *J. Power Sources* 249, 457–462. <https://doi.org/10.1016/j.jpowsour.2013.10.114>.
- Han, X., Ouyang, M., Lu, L., Li, J., Zheng, Y., Li, Z., 2014. A comparative study of commercial lithium ion battery cycle life in electrical vehicle: aging mechanism identification. *J. Power Sources* 251, 38–54. <https://doi.org/10.1016/j.jpowsour.2013.11.029>.
- Harlow, J.E., Glazier, S.L., Li, J., Dahn, J.R., 2018. Use of asymmetric average charge-and-average discharge-voltages as an indicator of the onset of unwanted lithium deposition in lithium-ion cells. *J. Electrochim. Soc.* 165, A3595–A3601. <https://doi.org/10.1149/2.0011816jes>.
- He, J., Bian, X., Liu, L., Wei, Z., Yan, F., 2020a. Comparative study of curve determination methods for incremental capacity analysis and state of health estimation of lithium-ion battery. *J. Energy Storage* 29, 101400. <https://doi.org/10.1016/j.est.2020.101400>.
- He, J., Wei, Z., Bian, X., Yan, F., 2020b. State-of-Health estimation of lithium-ion batteries using incremental capacity analysis based on voltage-capacity model. *IEEE Trans. Transp. Electrific.* 6, 417–426. <https://doi.org/10.1109/tte.2020.2994543>.
- Hsieh, A.G., Bhadra, S., Hertzberg, B.J., Gjeltema, P.J., Goy, A., Fleischer, J.W., Steingart, D.A., 2015. Electrochemical-acoustic time of flight: in operando correlation of physical dynamics with battery charge and health. *Energy Environ. Sci.* 8, 1569–1577. <https://doi.org/10.1039/C5EE00111K>.
- Hu, X., Feng, F., Liu, K., Zhang, L., Xie, J., Liu, B., 2019. State estimation for advanced battery management: key challenges and future trends. *Renew. Sustain. Energy Rev.* 114, 109334. <https://doi.org/10.1016/j.rser.2019.109334>.
- Hu, X., Jiang, H., Feng, F., Liu, B., 2020a. An enhanced multi-state estimation hierarchy for advanced lithium-ion battery management. *Appl. Energy* 257, 114019. <https://doi.org/10.1016/j.apenergy.2019.114019>.
- Hu, X., Jiang, H., Feng, F., Zou, C., 2018. A novel multi-scale Co-estimation framework of state of charge, state of health, and state of power for lithium-ion batteries, in: international conference on energy, ecology and environment (ICEEE 2018) and international conference on electric and intelligent vehicles (ICEEV 2018), DESTech transactions on environment, energy and earth sciences. Swinburne Univ Technol 1–8. <https://doi.org/10.12783/dteees/iceee2018/27824>. Melbourne, AUSTRALIA.
- Hu, X., Xu, L., Lin, X., Pecht, M., 2020b. Battery lifetime prognostics. *Joule* 4, 310–346. <https://doi.org/10.1016/j.joule.2019.11.018>.
- Hu, X., Zou, C., Zhang, C., Li, Y., 2017. Technological developments in batteries: a survey of principal roles, types, and management needs. *IEEE Power Energy Mag.* 15, 20–31. <https://doi.org/10.1109/mpe.2017.2708812>.
- Hua, Y., Cordoba-Arenas, A., Warner, N., Rizzoni, G., 2015. A multi time-scale state-of-charge and state-of-health estimation framework using nonlinear predictive filter for lithium-ion battery pack with passive balance control. *J. Power Sources* 280, 293–312. <https://doi.org/10.1016/j.jpowsour.2015.01.112>.
- Huang, J., Albero Blanquer, L., Bonefacino, J., Logan, E.R., Alves Dalla Corte, D., Delacourt, C., Gallant, B.M., Boles, S.T., Dahn, J.R., Tam, H.Y., Tarascon, J.M., 2020. Operando decoding of chemical and thermal events in commercial Na(Li)-ion cells via optical sensors. *Nat. Energy* 5, 674–683. <https://doi.org/10.1038/s41560-020-0665-y>.
- Jalkanen, K., Karppinen, J., Skogström, L., Laurila, T., Nisula, M., Vuorilehto, K., 2015. Cycle aging of commercial NMC/graphite pouch cells at different temperatures. *Appl. Energy* 154, 160–172. <https://doi.org/10.1016/j.apenergy.2015.04.110>.
- Jia, X., Zhang, C., Wang, L.Y., Zhang, L., Zhang, W., 2020. The degradation characteristics and mechanism of Li[Ni_{0.5}Co_{0.2}Mn_{0.3}]O₂ batteries at different temperatures and discharge current rates. *J. Electrochim. Soc.* 167, 020503. <https://doi.org/10.1149/1945-7111/ab61e9>.
- Jiang, B., Dai, H., Wei, X., 2020. Incremental capacity analysis based adaptive capacity estimation for lithium-ion battery considering charging condition. *Appl. Energy* 269, 115074. <https://doi.org/10.1016/j.apenergy.2020.115074>.
- Jiang, B., Dai, H., Wei, X., Xu, T., 2019a. Joint estimation of lithium-ion battery state of charge and capacity within an adaptive variable multi-timescale framework considering current measurement offset. *Appl. Energy* 253, 113619. <https://doi.org/10.1016/j.apenergy.2019.113619>.
- Jiang, J., Gao, Y., Zhang, C., Wang, Y., Zhang, W., Liu, S., 2019b. Online diagnostic method for health status of lithium-ion battery in electric vehicle. *Jixie Gongcheng Xuebao/Journal Mech. Eng.* 55. <https://doi.org/10.3901/JME.2019.20.060>.
- Jiang, Y., Jiang, J., Zhang, C., Zhang, W., Gao, Y., Guo, Q., 2017. Recognition of battery aging variations for LiFePO₄ batteries in 2nd use applications combining incremental capacity analysis and statistical approaches. *J. Power Sources* 360, 180–188. <https://doi.org/10.1016/j.jpowsour.2017.06.007>.
- Jiang, Y., Jiang, J., Zhang, C., Zhang, W., Gao, Y., Mi, C., 2019c. A Copula-based battery pack consistency modeling method and its application on the energy utilization efficiency estimation. *Energy* 189, 116219. <https://doi.org/10.1016/j.energy.2019.116219>.
- Johnen, M., Pitzen, S., Kampf, U., Kateri, M., Dechent, P., Sauer, D.U., 2021. Modeling long-term capacity degradation of lithium-ion batteries. *J. Energy Storage* 34, 1–15. <https://doi.org/10.1016/j.est.2020.102011>.
- Käbitz, S., Bernhard, J., Ecker, M., Yurdagel, Y., Emmermacher, B., André, D., Mitsch, T., Uwe, D., 2013. Cycle and calendar life study of a graphite|LiNi_{1/3}Mn_{1/3}Co_{1/3}O₂ Li-ion high energy system. Part A : full cell characterization. *J. Power Sources* 239, 572–583. <https://doi.org/10.1016/j.jpowsour.2013.03.045>.
- Kim, J., Chun, H., Kim, M., Yu, J., Kim, K., Kim, T., Han, S., 2019. Data-driven state of health estimation of Li-ion batteries with RPT-reduced experimental data. *IEEE Access* 7, 106987–106997. <https://doi.org/10.1109/access.2019.2932719>.
- Kim, T., Makwana, D., Adhikaree, A., Vagdoda, J.S., Lee, Y., 2018. Cloud-based battery condition monitoring and fault diagnosis platform for large-scale lithium-ion battery energy storage systems. *Energies* 11, 1–15. <https://doi.org/10.3390/en11010125>.
- Kim, T., Qiao, W., Qu, L., 2013. Online SOC and SOH estimation for multicell lithium-ion batteries based on an adaptive hybrid battery model and sliding-mode observer. 2013 IEEE Energy Convers. Congr. Expo 292–298. <https://doi.org/10.1109/ECCE.2013.6646714>.
- Klass, V., Behm, M., Lindbergh, G., 2014. A support vector machine-based state-of-health estimation method for lithium-ion batteries under electric vehicle operation. *J. Power Sources* 270, 262–272. <https://doi.org/10.1016/j.jpowsour.2014.07.116>.
- Klein, M., Tong, S., Park, J.W., 2016. In-plane nonuniform temperature effects on the performance of a large-format lithium-ion pouch cell. *Appl. Energy* 165, 639–647. <https://doi.org/10.1016/j.apenergy.2015.11.090>.
- Knehr, K.W., Bommier, C., Davies, G., Kim, A., Steingart, D.A., Knehr, K.W., Hodson, T., Bommier, C., Davies, G., Kim, A., 2018. Understanding full-cell evolution and non-chemical electrode crosstalk of Li-ion batteries understanding full-cell evolution and non-chemical electrode crosstalk of Li-ion batteries. *Joule* 2, 1146–1159. <https://doi.org/10.1016/j.joule.2018.03.016>.

- Koch, S., Birke, K.P., Kuhn, R., 2018. Fast thermal runaway detection for lithium-ion cells in large scale traction batteries. *Batteries* 4, 1–11. <https://doi.org/10.3390/batteries4020016>.
- Kwon, S., Han, D., Hyeok, J., Lim, J., Lee, S., Kim, J., 2020. Remaining-useful-life prediction via multiple linear regression and recurrent neural network re reflecting degradation information of 20Ah LiNi_xMn_yCo_{1-x-y}O₂ pouch cell. *J. Electroanal. Chem.* 858, 113729. <https://doi.org/10.1016/j.jelechem.2019.113729>.
- Ladpli, P., Kopsaftopoulos, F., Chang, F., 2018. Estimating state of charge and health of lithium-ion batteries with guided waves using built-in piezoelectric sensors/actuators. *J. Power Sources* 384, 342–354. <https://doi.org/10.1016/j.jpowsour.2018.02.056>.
- Lee, S., Mohtat, P., Siegel, J.B., Stefanopoulou, A.G., Lee, J.W., Lee, T.K., 2020. Estimation error bound of battery electrode parameters with limited data window. *IEEE Trans. Ind. Informatics* 16, 3376–3386. <https://doi.org/10.1109/TII.2019.2952066>.
- Lee, S., Siegel, J.B., Stefanopoulou, A.G., Lee, J.W., Lee, T.K., 2018. Comparison of individual-electrode state of health estimation methods for lithium ion battery. In: ASME 2018 Dynamic Systems and Control Conference, DSAC 2018, pp. 1–10. <https://doi.org/10.1115/DSCC2018-9014>.
- Li, J., Lyu, C., Wang, L., Zhang, L., Li, C., 2014a. Remaining capacity estimation of Li-ion batteries based on temperature sample entropy and particle filter. *J. Power Sources* 268, 895–903. <https://doi.org/10.1016/j.jpowsour.2014.06.133>.
- Li, K., Wei, F., Tseng, K.J., Soong, B.-H., 2018. A practical lithium-ion battery model for state of energy and voltage responses prediction incorporating temperature and ageing effects. *IEEE Trans. Ind. Electron.* 65, 6696–6708. <https://doi.org/10.1109/TIE.2017.2779411>.
- Li, S., He, H., Li, J., 2019a. Big data driven lithium-ion battery modeling method based on SDAE-ELM algorithm and data pre-processing technology. *Appl. Energy* 242, 1259–1273. <https://doi.org/10.1016/j.apenergy.2019.03.154>.
- Li, S.E., Wang, B., Peng, H., Hu, X., 2014b. An electrochemistry-based impedance model for lithium-ion batteries. *J. Power Sources* 258, 9–18. <https://doi.org/10.1016/j.jpowsour.2014.02.045>.
- Li, W., Rentemeister, M., Baedea, J., Jöst, D., Schulte, D., Sauer, D.U., 2020. Digital twin for battery systems: cloud battery management system with online state-of-charge and state-of-health estimation. *J. Energy Storage* 30, 101557. <https://doi.org/10.1016/j.est.2020.101557>.
- Li, X., Jiang, J., Wang, L.Y., Chen, D., Zhang, Y., Zhang, C., 2016. A capacity model based on charging process for state of health estimation of lithium ion batteries. *Appl. Energy* 177, 537–543. <https://doi.org/10.1016/j.apenergy.2016.05.109>.
- Li, X., Wang, Z., Zhang, L., 2019b. Co-estimation of capacity and state-of-charge for lithium-ion batteries in electric vehicles. *Energy* 174, 33–44. <https://doi.org/10.1016/j.energy.2019.02.147>.
- Li, Y., Liu, K., Foley, A.M., Zülke, A., Berecibar, M., Nanini-Maury, E., Van Mierlo, J., Hoster, H.E., 2019c. Data-driven health estimation and lifetime prediction of lithium-ion batteries: a review. *Renew. Sustain. Energy Rev.* 113 <https://doi.org/10.1016/j.rser.2019.109254>.
- Lipu, M.S.H., Hannan, M.A., Hussain, A., Hoque, M.M., Ker, P.J., Saad, M.H.M., Ayob, A., 2018. A review of state of health and remaining useful life estimation methods for lithium-ion battery in electric vehicles: challenges and recommendations. *J. Clean. Prod.* 205, 115–133. <https://doi.org/10.1016/j.jclepro.2018.09.065>.
- Liu, D., Zhou, J., Pan, D., Peng, Y., Peng, X., 2015. Lithium-ion battery remaining useful life estimation with an optimized Relevance Vector Machine algorithm with incremental learning. *Meas. J. Int. Meas. Confed.* 63, 143–151. <https://doi.org/10.1016/j.measurement.2014.11.031>.
- Love, C.T., Virji, M.B.V., Rocheleau, R.E., Swider-lyons, K.E., 2014. State-of-health monitoring of 18650 4S packs with a single-point impedance diagnostic. *J. Power Sources* 266, 512–519. <https://doi.org/10.1016/j.jpowsour.2014.05.033>.
- Lu, C., Tao, L., Fan, H., 2014. Li-ion battery capacity estimation : a geometrical approach. *J. Power Sources* 261, 141–147. <https://doi.org/10.1016/j.jpowsour.2014.03.058>.
- Lu, J., Li, X., Lei, H., Liu, Y., Xiong, R., 2019. Remaining useful life prediction driven by multi-source data for batteries in electric vehicles. *DEStech Transactions on Environment, Energy and Earth Sciences* 199–202. <https://doi.org/10.12783/dtees/iceee2019/31807>.
- Lucu, M., Martínez-laserna, E., Gandiaga, I., Liu, K., Camblong, H., Widanage, W.D., 2020. Data-driven nonparametric Li-ion battery ageing model aiming at learning from real operation data – Part A : storage operation. *J. Energy Storage* 30, 101409. <https://doi.org/10.1016/j.est.2020.101409>.
- Lyu, C., Song, Y., Zheng, J., Luo, W., Hinds, G., Li, J., Wang, L., 2019. In situ monitoring of lithium-ion battery degradation using an electrochemical model. *Appl. Energy* 250, 685–696. <https://doi.org/10.1016/j.apenergy.2019.05.038>.
- Ma, Z., Wang, Z., Xiong, R., Jiang, J., 2018. A mechanism identification model based state-of-health diagnosis of lithium-ion batteries for energy storage applications. *J. Clean. Prod.* 193, 379–390. <https://doi.org/10.1016/j.jclepro.2018.05.074>.
- Marongiu, A., Nlandi, N., Rong, Y., Sauer, D.U., 2016. On-board capacity estimation of lithium iron phosphate batteries by means of half-cell curves. *J. Power Sources* 324, 158–169. <https://doi.org/10.1016/j.jpowsour.2016.05.041>.
- Merla, Y., Wu, B., Yu, V., Brandon, N.P., Martinez-botás, R.F., Offer, G.J., 2016a. Novel application of differential thermal voltammetry as an in-depth state-of-health diagnosis method for lithium-ion batteries. *J. Power Sources* 307, 308–319. <https://doi.org/10.1016/j.jpowsour.2015.12.122>.
- Merla, Y., Wu, B., Yu, V., Brandon, N.P., Martinez-botás, R.F., Offer, G.J., 2016b. Extending battery life : a low-cost practical diagnostic technique for lithium-ion batteries. *J. Power Sources* 331, 224–231. <https://doi.org/10.1016/j.jpowsour.2016.09.008>.
- Mohtat, P., Lee, S., Siegel, J.B., Stefanopoulou, A.G., 2019. Towards better estimability of electrode-specific state of health: decoding the cell expansion. *J. Power Sources* 427, 101–111. <https://doi.org/10.1016/j.jpowsour.2019.03.104>.
- Mousavi, M., Taskhiri, M.S., Holloway, D., Olivier, J.C., Turner, P., 2020. Feature extraction of wood-hole defects using empirical mode decomposition of ultrasonic signals. *NDT E Int.* 114, 102282. <https://doi.org/10.1016/j.ndteint.2020.102282>.
- Mukhopadhyay, A., Sheldon, B.W., 2014. Deformation and stress in electrode materials for Li-ion batteries. *Prog. Mater. Sci.* 63, 58–116. <https://doi.org/10.1016/j.pmatsci.2014.02.001>.
- Naha, A., Han, S., Agarwal, S., Guha, A., Khandelwal, A., Tagade, P., Hariharan, K.S., Kolake, S.M., Yoon, J., Oh, B., 2020. An incremental voltage difference based technique for online state of health estimation of Li-ion batteries. *Sci. Rep.* 10, 1–11. <https://doi.org/10.1038/s41598-020-66424-9>.
- Novais, S., Nascimento, M., Grande, L., Domingues, M.F., Antunes, P., Alberto, N., Leitão, C., Oliveira, R., Koch, S., Kim, G.T., Passerini, S., Pinto, J., 2016. Internal and external temperature monitoring of a li-ion battery with fiber bragg grating sensors. *Sensors* 16, 1–9. <https://doi.org/10.3390/s16091394>.
- Nuhic, A., Terzimehic, T., Soczka-guth, T., Buchholz, M., Dietmayer, K., 2013. Health diagnosis and remaining useful life prognostics of lithium-ion batteries using data-driven methods q. *J. Power Sources* 239, 680–688. <https://doi.org/10.1016/j.jpowsour.2012.11.146>.
- Oh, K.Y., Siegel, J.B., Seconde, L., Kim, S.U., Samad, N.A., Qin, J., Anderson, D., Garikipati, K., Knobloch, A., Epureanu, B.I., Monroe, C.W., Stefanopoulou, A., 2014. Rate dependence of swelling in lithium-ion cells. *J. Power Sources* 267, 197–202. <https://doi.org/10.1016/j.jpowsour.2014.05.039>.
- Pastor-Fernández, C., Uddin, K., Chouchelamane, G.H., Widanage, W.D., Marco, J., 2017. A comparison between electrochemical impedance spectroscopy and incremental capacity-differential voltage as Li-ion diagnostic techniques to identify and quantify the effects of degradation modes within battery management systems. *J. Power Sources* 360, 301–318. <https://doi.org/10.1016/j.jpowsour.2017.03.042>.
- Paul, S., Diegelmann, C., Kabza, H., Tillmetz, W., 2013. Analysis of ageing inhomogeneities in lithium-ion battery systems. *J. Power Sources* 239, 642–650. <https://doi.org/10.1016/j.jpowsour.2013.01.068>.
- Peabody, C., Arnold, C.B., 2011. The role of mechanically induced separator creep in lithium-ion battery capacity fade. *J. Power Sources* 196, 8147–8153. <https://doi.org/10.1016/j.jpowsour.2011.05.023>.
- Petzl, M., Danzer, M.A., 2014. Nondestructive detection, characterization, and quantification of lithium plating in commercial lithium-ion batteries. *J. Power Sources* 254, 80–87. <https://doi.org/10.1016/j.jpowsour.2013.12.060>.
- Petzl, M., Kasper, M., Danzer, M.A., 2015. Lithium plating in a commercial lithium-ion battery - a low-temperature aging study. *J. Power Sources* 275, 799–807. <https://doi.org/10.1016/j.jpowsour.2014.11.065>.
- Popp, H., Koller, M., Jahn, M., Bergmann, A., 2020. Mechanical methods for state determination of Lithium-Ion secondary batteries: a review. *J. Energy Storage* 32, 101859. <https://doi.org/10.1016/j.est.2020.101859>.
- Prasad, G.K., Rahn, C.D., 2013. Model based identification of aging parameters in lithium ion batteries. *J. Power Sources* 232, 79–85. <https://doi.org/10.1016/j.jpowsour.2013.01.041>.
- Raghavan, A., Kiesel, P., Sommer, L.W., Schwartz, J., Lochbaum, A., Hegyi, A., Schuh, A., Arakaki, K., Saha, B., Ganguli, A., Kim, K.H., Kim, C.A., Hah, H.J., Kim, S.K., Hwang, G.O., Chung, G.C., Choi, B., Alamgir, M., 2017. Embedded fiber-optic sensing for accurate internal monitoring of cell state in advanced battery management systems part 1: cell embedding method and performance. *J. Power Sources* 341, 466–473. <https://doi.org/10.1016/j.jpowsour.2016.11.104>.
- Raijmakers, L.H.J., Danilov, D.L., Eichel, R.A., Notten, P.H.L., 2019. A review on various temperature-indication methods for Li-ion batteries. *Appl. Energy* 240, 918–945. <https://doi.org/10.1016/j.apenergy.2019.02.078>.
- Richardson, R.R., Birk, C.R., Osborne, M.A., Howey, D.A., 2019. Gaussian process regression for in situ capacity estimation of Lithium-ion batteries. *IEEE Trans. Ind. Informatics* 15, 127–138. <https://doi.org/10.1109/TII.2018.2794997>.
- Samad, N.A., Kim, Y., Siegel, J.B., Stefanopoulou, A.G., 2016. Battery capacity fading estimation using a force-based incremental capacity analysis. *J. Electrochem. Soc.* 163, A1584–A1594. <https://doi.org/10.1149/2.0511608jes>.
- Sarasketa-Zabala, E., Agüesse, F., Villarreal, I., Rodriguez-Martinez, L.M., López, C.M., Kubiak, P., 2015. Understanding lithium inventory loss and sudden performance fade in cylindrical cells during cycling with deep-discharge steps. *J. Phys. Chem. C* 119, 896–906. <https://doi.org/10.1021/jpc050071d>.
- Sauersteig, D., Hanselmann, N., Arzberger, A., Reinshagen, H., Ivanov, S., Bund, A., 2018. Electrochemical-mechanical coupled modeling and parameterization of swelling and ionic transport in lithium-ion batteries. *J. Power Sources* 378, 235–247. <https://doi.org/10.1016/j.jpowsour.2017.12.044>.
- Saxena, S., Hendricks, C., Pecht, M., 2016. Cycle life testing and modeling of graphite/LiCoO₂ cells under different state of charge ranges. *J. Power Sources* 327, 394–400. <https://doi.org/10.1016/j.jpowsour.2016.07.057>.
- Schiffer, Z.J., Cannarella, J., Arnold, C.B., 2016. Strain derivatives for practical charge rate characterization of lithium ion electrodes. *J. Electrochem. Soc.* 163, A427–A433. <https://doi.org/10.1149/2.0091603jes>.
- Schuster, Simon F., Bach, T., Fleder, E., Müller, J., Brand, M., Sextl, G., Jossen, A., 2015a. Nonlinear aging characteristics of lithium-ion cells under different operational conditions. *J. Energy Storage* 1, 44–53. <https://doi.org/10.1016/j.est.2015.05.003>.
- Schuster, Simon F., Brand, M.J., Berg, P., Gleissenberger, M., Jossen, A., 2015b. Lithium-ion cell-to-cell variation during battery electric vehicle operation. *J. Power Sources* 297, 242–251. <https://doi.org/10.1016/j.jpowsour.2015.08.001>.
- Schweiger, H., Obeidi, O., Komesker, O., Raschke, A., Schiemann, M., Zehner, C., Gehnen, M., Keller, M., Birke, P., 2010. Comparison of several methods for

- determining the internal resistance of lithium ion cells. Sensors 5604–5625. <https://doi.org/10.3390/s100605604>.
- Severson, K.A., Attia, P.M., Jin, N., Perkins, N., Jiang, B., Yang, Z., Chen, M.H., Aykol, M., Herring, P.K., Fragedakis, D., Bazant, M.Z., Harris, S.J., Chueh, W.C., Braatz, R.D., 2019. Data-driven prediction of battery cycle life before capacity degradation. *Nat. Energy* 4, 383–391. <https://doi.org/10.1038/s41560-019-0356-8>.
- Shibagaki, T., Merla, Y., Gregory, J.O., 2018. Tracking degradation in lithium iron phosphate batteries using differential thermal voltammetry. *J. Power Sources* 374, 188–195. <https://doi.org/10.1016/j.jpowsour.2017.11.011>.
- Sihvo, J., Messo, T., Roinila, T., Luhtala, R., Stroe, D.I., 2018. Online identification of internal impedance of Li-ion battery cell using ternary-sequence injection. In: 2018 IEEE Energy Conversion Congress and Exposition, ECCE 2018, pp. 2705–2711. <https://doi.org/10.1109/ECCE.2018.8558147>.
- Sihvo, J., Roinila, T., Stroe, D.I., 2020a. Broadband impedance measurement of lithium-ion battery in the presence of nonlinear distortions. *Energies* 13, 1–15. <https://doi.org/10.3390/en13102493>.
- Sihvo, J., Stroe, D.I., Messo, T., Roinila, T., 2020b. Fast approach for battery impedance identification using pseudo-random sequence signals. *IEEE Trans. Power Electron.* 35, 2548–2557. <https://doi.org/10.1109/TPEL.2019.2924286>.
- Sommer, L.W., Raghavan, A., Kiesel, P., Saha, B., Schwartz, J., Lochbaum, A., Ganguli, A., Bae, C.-J., Alamgir, M., 2015. Monitoring of intercalation stages in lithium-ion cells over charge-discharge cycles with fiber optic sensors. *J. Electrochem. Soc.* 162, A2664–A2669. <https://doi.org/10.1149/2.0361514jes>.
- Song, L., Zhang, K., Liang, T., Han, X., Zhang, Y., 2020. Intelligent state of health estimation for lithium-ion battery pack based on big data analysis. *J. Energy Storage* 32, 101836. <https://doi.org/10.1016/j.est.2020.101836>.
- Song, Y., Liu, D., Peng, Y., 2019. Series-connected lithium-ion battery pack health modeling with cell inconsistency evaluation. 2019 IEEE Int. Instrum. Meas. Technol. Conf. 1–6.
- Sood, B., Osterman, M., Pecht, M., 2013. Health monitoring of lithium-ion batteries. In: Proceedings - 10th Annual IEEE Symposium on Product Compliance Engineering, ISPCE 2013, pp. 3–8. <https://doi.org/10.1109/ISPCE.2013.6664165>.
- Su, L., Wang, Z., Ren, Y., 2019. A novel two-steps method for estimation of the capacity imbalance among in-pack cells. *J. Energy Storage* 26, 101031. <https://doi.org/10.1016/j.est.2019.101031>.
- Sun, H., Zhu, J., 2020. Nondestructive evaluation of steel-concrete composite structure using high-frequency ultrasonic guided wave. *Ultrasonics* 103, 106096. <https://doi.org/10.1016/j.ultras.2020.106096>.
- Sun, S., Guan, T., Cheng, X., Zuo, P., Gao, Y., Du, C., Yin, G., 2018. Accelerated aging and degradation mechanism of LiFePO₄/graphite batteries cycled at high discharge rates. *RSC Adv.* 8, 25695–25703. <https://doi.org/10.1039/c8ra04074e>.
- Sun, S., Guan, T., Shen, B., Leng, K., Gao, Y., Cheng, X., Yin, G., 2017. Changes of degradation mechanisms of LiFePO₄/graphite batteries cycled at different ambient temperatures. *Electrochim. Acta* 237, 248–258. <https://doi.org/10.1016/j.electacta.2017.03.158>.
- Tagade, P., Hariharan, K.S., Ramachandran, S., Khandelwal, A., Naha, A., Kolake, S.M., Han, S.H., 2020. Deep Gaussian process regression for lithium-ion battery health prognosis and degradation mode diagnosis. *J. Power Sources* 445, 227281. <https://doi.org/10.1016/j.jpowsour.2019.227281>.
- Tian, H., Qin, P., Li, K., Zhao, Z., 2020a. A review of the state of health for lithium-ion batteries research status and suggestions. *J. Clean. Prod.* <https://doi.org/10.1016/j.jclepro.2020.120813>.
- Tian, J., Xiong, R., Shen, W., 2020b. State-of-Health estimation based on differential temperature for lithium ion batteries. *IEEE Trans. Power Electron.* 35, 10363–10373. <https://doi.org/10.1109/TPEL.2020.2978493>.
- Tian, J., Xiong, R., Shen, W., 2019. A review on state of health estimation for lithium ion batteries in photovoltaic systems. *eTransportation* 2, 100028. <https://doi.org/10.1016/j.etrans.2019.100028>.
- Tomaszewska, A., Chu, Z., Feng, X., O'Kane, S., Liu, X., Chen, J., Ji, C., Endler, E., Li, R., Liu, L., Li, Y., Zheng, S., Vetterlein, S., Gao, M., Du, J., Parkes, M., Ouyang, M., Marinescu, M., Offer, G., Wu, B., 2019. Lithium-ion battery fast charging: a review. *eTransportation* 1, 100011. <https://doi.org/10.1016/j.etrans.2019.100011>.
- Torai, S., Nakagomi, M., Yoshitake, S., Yamaguchi, S., Oyama, N., 2016. State-of-health estimation of LiFePO₄/graphite batteries based on a model using differential capacity. *J. Power Sources* 306, 62–69. <https://doi.org/10.1016/j.jpowsour.2015.11.070>.
- Waag, W., Fleischer, C., Sauer, D.U., 2014. Critical review of the methods for monitoring of lithium-ion batteries in electric and hybrid vehicles. *J. Power Sources* 258, 321–339. <https://doi.org/10.1016/j.jpowsour.2014.02.064>.
- Waag, W., Fleischer, C., Sauer, D.U., 2013. Adaptive on-line prediction of the available power of lithium-ion batteries. *J. Power Sources* 242, 548–559. <https://doi.org/10.1016/j.jpowsour.2013.05.111>.
- Waldmann, T., Wilka, M., Kasper, M., Fleischhammer, M., Wohlfahrt-mehrens, M., 2014. Temperature dependent ageing mechanisms in Lithium-ion batteries - a Post-Mortem study. *J. Power Sources* 262, 129–135. <https://doi.org/10.1016/j.jpowsour.2014.03.112>.
- Wang, D., Miao, Q., Pecht, M., 2013. Prognostics of lithium-ion batteries based on relevance vectors and a conditional three-parameter capacity degradation model. *J. Power Sources* 239, 253–264. <https://doi.org/10.1016/j.jpowsour.2013.03.129>.
- Wang, H., Frisco, S., Gottlieb, E., Yuan, R., Whitacre, J.F., 2019. Capacity degradation in commercial Li-ion cells: the effects of charge protocol and temperature. *J. Power Sources* 426, 67–73. <https://doi.org/10.1016/j.jpowsour.2019.04.034>.
- Wang, L., Pan, C., Liu, L., Cheng, Y., Zhao, X., 2016. On-board state of health estimation of LiFePO₄ battery pack through differential voltage analysis. *Appl. Energy* 168, 465–472. <https://doi.org/10.1016/j.apenergy.2016.01.125>.
- Wang, Y., Tian, J., Sun, Z., Wang, L., Xu, R., Li, M., Chen, Z., 2020. A comprehensive review of battery modeling and state estimation approaches for advanced battery management systems. *Renew. Sustain. Energy Rev.* 131, 110015. <https://doi.org/10.1016/j.rser.2020.110015>.
- Watanabe, S., Kinoshita, M., Hosokawa, T., Morigaki, K., Nakura, K., 2014. Capacity fading of LiAl_xNi_{1-x}CoxO₂ cathode for lithium-ion batteries during accelerated calendar and cycle life tests (effect of depth of discharge in charge-discharge cycling on the suppression of the micro-crack generation of LiAl_xNi_{1-x}CoxO₂ part). *J. Power Sources* 260, 50–56. <https://doi.org/10.1016/j.jpowsour.2014.02.103>.
- Widanage, W.D., Barai, A., Chouchelamane, G.H., Uddin, K., McGordon, A., Marco, J., Jennings, P., 2016a. Design and use of multisine signals for Li-ion battery equivalent circuit modelling. Part 2: model estimation. *J. Power Sources* 324, 61–69. <https://doi.org/10.1016/j.jpowsour.2016.05.014>.
- Widanage, W.D., Barai, A., Chouchelamane, G.H., Uddin, K., McGordon, A., Marco, J., Jennings, P., 2016b. Design and use of multisine signals for Li-ion battery equivalent circuit modelling. Part 1: signal design. *J. Power Sources* 324, 70–78. <https://doi.org/10.1016/j.jpowsour.2016.05.015>.
- Woody, M., Arbabzadeh, M., Lewis, G.M., Keoleian, G.A., Stefanopoulou, A., 2020. Strategies to limit degradation and maximize Li-ion battery service lifetime - critical review and guidance for stakeholders. *J. Energy Storage* 28, 101231. <https://doi.org/10.1016/j.est.2020.101231>.
- Wu, B., Yu, V., Merla, Y., Martinez-botás, R.F., Brandon, N.P., Offer, G.J., 2015. Differential thermal voltammetry for tracking of degradation in lithium-ion batteries. *J. Power Sources* 273, 495–501. <https://doi.org/10.1016/j.jpowsour.2014.09.127>.
- Wu, J., Wang, Y., Zhang, X., Chen, Z., 2016a. A novel state of health estimation method of Li-ion battery using group method of data handling. *J. Power Sources* 327, 457–464. <https://doi.org/10.1016/j.jpowsour.2016.07.065>.
- Wu, L., Fu, X., Guan, Y., 2016b. Review of the remaining useful life prognostics of vehicle lithium-ion batteries using data-driven methodologies. *Appl. Sci.* <https://doi.org/10.3390/app6060166>.
- Wu, X., Wang, W., Du, J., 2020. Effect of charge rate on capacity degradation of LiFePO₄ power battery at low temperature. *Int. J. Energy Res.* 44, 1775–1788. <https://doi.org/10.1002/er.5022>.
- Wu, Y., Jossen, A., 2018. Entropy-induced temperature variation as a new indicator for state of health estimation of lithium-ion cells. *Electrochim. Acta* 276, 370–376. <https://doi.org/10.1016/j.electacta.2018.04.203>.
- Wu, Y., Wang, Y., Yung, W.K.C., Pecht, M., 2019. Ultrasonic health monitoring of lithium-ion batteries. *Electronics* 8, 751. <https://doi.org/10.3390/electronics8070751>.
- Xia, Z., Qahouq, J.A.A., 2018. State-of-health indication method for Li-Ion batteries. In: Conf. Proc. - IEEE Appl. Power Electron. Conf. Expo. - APEC 2018-March, 1829–1833. <https://doi.org/10.1109/APEC.2018.8341265>.
- Xiao, D., Fang, G., Liu, S., Yuan, S., Ahmed, R., Habibi, S., Emadi, A., 2020. Reduced-coupling coestimation of SOC and SOH for lithium-ion batteries based on convex optimization. *IEEE Trans. Power Electron.* 35, 12332–12346. <https://doi.org/10.1109/TPEL.2020.2984248>.
- Xiong, R., Li, L., Tian, J., 2018. Towards a smarter battery management system: a critical review on battery state of health monitoring methods. *J. Power Sources* 405, 18–29. <https://doi.org/10.1016/j.jpowsour.2018.10.019>.
- Xiong, R., Zhang, Y., Wang, J., He, H., Peng, S., Pecht, M., 2019. Lithium-ion battery health prognosis based on a real battery management system used in electric vehicles. *IEEE Trans. Veh. Technol.* 68, 4110–4121. <https://doi.org/10.1109/TVT.2018.2864688>.
- Xu, J., Mei, X., Wang, X., Fu, Y., Zhao, Y., Wang, J., 2020. A relative state of health estimation method based on wavelet analysis for lithium-ion battery cells. *IEEE Trans. Ind. Electron.* 46 <https://doi.org/10.1109/tie.2020.3001836>, 1–1.
- Xuan, D., Shi, Z., Chen, J., Zhang, C., Wang, Y., 2020. Real-time estimation of state-of-charge in lithium-ion batteries using improved central difference transform method. *J. Clean. Prod.* 252, 119787. <https://doi.org/10.1016/j.jclepro.2019.119787>.
- Yan, L., Bingham, C., Cruz-Manzo, S., Cui, D., Lv, Y., 2020. Battery impedance measurement using pseudo random binary sequences. In: 2020 IEEE Student Conference on Electric Machines and Systems, SCEMS 2020, pp. 686–691. <https://doi.org/10.1109/SCEMS48876.2020.9352336>.
- Yang, D., Wang, Y., Pan, R., Chen, R., Chen, Z., 2018a. State-of-health estimation for the lithium-ion battery based on support vector regression. *Appl. Energy* 227, 273–283. <https://doi.org/10.1016/j.apenergy.2017.08.096>.
- Yang, D., Zhang, X., Pan, R., Wang, Y., Chen, Z., 2018b. A novel Gaussian process regression model for state-of-health estimation of lithium-ion battery using charging curve. *J. Power Sources* 384, 387–395. <https://doi.org/10.1016/j.jpowsour.2018.03.015>.
- Yang, F., Wang, D., Zhao, Y., Tsui, K.L., Bae, S.J., 2018c. A study of the relationship between coulombic efficiency and capacity degradation of commercial lithium-ion batteries. *Energy* 145, 486–495. <https://doi.org/10.1016/j.energy.2017.12.144>.
- Yang, J., Xia, B., Huang, W., Fu, Y., Mi, C., 2018d. Online state-of-health estimation for lithium-ion batteries using constant-voltage charging current analysis. *Appl. Energy* 212, 1589–1600. <https://doi.org/10.1016/j.apenergy.2018.01.010>.
- Yang, X.G., Leng, Y., Zhang, G., Ge, S., Wang, C.Y., 2017. Modeling of lithium plating induced aging of lithium-ion batteries: transition from linear to nonlinear aging. *J. Power Sources* 360, 28–40. <https://doi.org/10.1016/j.jpowsour.2017.05.110>.
- You, G., Park, S., Oh, D., 2016. Real-time state-of-health estimation for electric vehicle batteries : a data-driven approach. *Appl. Energy* 176, 92–103. <https://doi.org/10.1016/j.apenergy.2016.05.051>.
- Yu, J., Mo, B., Tang, D., Yang, J., Wan, J., Liu, J., 2017. Indirect state-of-health estimation for lithium-ion batteries under randomized use. *Energies* 10, 1–19. <https://doi.org/10.3390/en1012202>.

- Zeng, W., Qi, S., Liu, L., Yao, F., 2020. An quantitative inspection method for internal defects based on laser ultrasonic technology. *Optik (Stuttgart)*. 216, 164873. <https://doi.org/10.1016/j.ijleo.2020.164873>.
- Zhang, C., Wang, Y., Gao, Y., Wang, F., Mu, B., Zhang, W., 2019. Accelerated fading recognition for lithium-ion batteries with Nickel-Cobalt-Manganese cathode using quantile regression method. *Appl. Energy* 256, 113841. <https://doi.org/10.1016/j.apenergy.2019.113841>.
- Zhang, J., Lee, J., 2011. A review on prognostics and health monitoring of Li-ion battery. *J. Power Sources* 196, 6007–6014. <https://doi.org/10.1016/j.jpowsour.2011.03.101>.
- Zhang, W., Shi, W., Ma, Z., 2015. Adaptive unscented Kalman filter based state of energy and power capability estimation approach for lithium-ion battery. *J. Power Sources* 289, 50–62. <https://doi.org/10.1016/j.jpowsour.2015.04.148>.
- Zhang, X., Wang, Y., Liu, C., Chen, Z., 2018. A novel approach of battery pack state of health estimation using artificial intelligence optimization algorithm. *J. Power Sources* 376, 191–199. <https://doi.org/10.1016/j.jpowsour.2017.11.068>.
- Zheng, Y., Wang, J., Qin, C., Lu, L., Han, X., Ouyang, M., 2019. A novel capacity estimation method based on charging curve sections for lithium-ion batteries in electric vehicles. *Energy* 185, 361–371. <https://doi.org/10.1016/j.energy.2019.07.059>.
- Zhou, X., Stein, J.L., Ersal, T., 2017. Battery state of health monitoring by estimation of the number of cyclable Li-ions. *Contr. Eng. Pract.* 66, 51–63. <https://doi.org/10.1016/j.conengprac.2017.05.009>.